The long-term trends of global land precipitation in GFDL's CM4 and ESM4 climate models

Yanda Zhang[1], Thomas R. Knutson[2], Elena Shevliakova[2], and David Paynter[2]

[1] Atmospheric and Oceanic Sciences Program, Princeton University, Princeton, New Jersey

[2] NOAA/Geophysical Fluid Dynamics Laboratory, Princeton, New Jersey

Corresponding author: Yanda Zhang, yz6753@princeton.edu and Thomas R. Knutson, tom.knutson@noaa.gov

1

Abstract

Historical precipitation and temperature trends and variations over global land regions are compared with simulations of two climate models focusing on grid points with substantial observational coverage from the early 20th century. Potential mechanisms for the differences between modeled and observed trends are investigated using subsets of historical forcings, including ones using only anthropogenic greenhouse gases or aerosols, and simulations forced with the observed sea surface temperature and sea ice distribution. For century-scale (1915–2014) precipitation trends, underestimated increasing or unrealistic decreasing trends are found in the models over the extratropical Northern Hemisphere. The temporal evolution of key discrepancies between the observations and simulations indicates: (1) for averages over 15°–45° N, while there is not a significant trend in observations, both models simulate reduced precipitation from 1940 to 2014; (2) for 45°–80° N: observations suggest sizable precipitation increases while models do not show a significant increase particularly during ~1950–1980. The timing of differences between models and observations suggesting a key role for aerosols in these dry trend biases over the extratropical Northern Hemisphere. (3) for 15°S–15°N, the observed multidecadal decrease over tropical west Africa (1950-1980) is roughly only captured by simulations forced with observed sea surface temperature; and (4) in the all-forcing runs, the model with higher global climate sensitivity, simulates increasing trends of temperature and precipitation over lands north of 45°N, that are significantly stronger than the lower-sensitivity model and more consistent with the observed increases. Thus, underestimated greenhouse gas-induced warming—particularly in the lower sensitivity model—may be another important factor, besides aerosols, contributing to the modeled biases in precipitation trends.

1. Introduction

Precipitation is one of the key elements of the Earth system, serving as a determinant shaping the climate zones, biome distribution, and the ecosystem. Changes in regional precipitation are a critical driver of flood and drought risks, affecting the environment (land aridity, water resources, vegetation variation, etc.), and human society (agriculture,

2

economics, and public safety). Thus, a thorough understanding of changes in precipitation is critical for ecological studies and societal decisions (IPCC. 2014).

Previous studies show that precipitation has changed over much of the globe in association with observed global warming and other climate changes (Trenberth, 2011; Hartmann et al., 2013). Analysis of precipitation observations and model simulations suggest that some observed changes in regional or zonally averaged precipitation can be attributed to anthropogenic forcing (Zhang et al. 2007; Andrews et al. 2010; Liu et al. 2013; Wilcox et al. 2013; Knutson and Zeng 2018). Global warming influences the hydrological cycle and precipitation patterns (Held and Soden, 2006; Marvel and Bonfils, 2013) in part via the Clausius–Clapeyron (CC) relationship, through which lower-tropospheric water vapor increases with temperature. As a consequence of the increasing lower-tropospheric water vapor, the changes in water vapor transport and the pattern of evaporation minus precipitation lead to the changes in precipitation that largely follows a "wet-get-wetter, dry-get-drier" relationship, in the absence of other influences (Held and Soden 2006; Zhang et al. 2007; Min et al. 2008; Chou et al. 2009; Fyfe et al. 2012).

In the fifth and sixth IPCC assessment reports (AR5, IPCC 2013; AR6, IPCC 2021) and underlying studies, changes in the global water cycle and precipitation at various temporal-spatial scales are demonstrated to be related to anthropogenic forcings in aggregate, including the anthropogenic aerosols (AA) and greenhouse gases (GHGs) (Zhang et al., 2007; Andrews et al., 2010; Liu et al., 2013; Marvel et al., 2013; Wilcox et al., 2013; Collins et al., 2013; Knutson and Zeng, 2018; Douville et al., 2021). Global mean precipitation is indicated to increase with global temperature at a rate of 1–3% $°C^{-1}$ explained by the fast atmospheric adjustments and slow responses to radiative forcings from GHGs and AAs (Andrews et al., 2010; Bala et al., 2010; Cao et al., 2012; Fläschner et al., 2016; Samset et al., 2016). Global mean precipitation is estimated by GCMs to increase by 2.0–4.6% after the removal of the present-day AA emissions, attributed to sulphate aerosol (Samset et al., 2018). Over the northern hemisphere (NH), station observations show decreasing trend during ~1950–1980 and recovery since, due to the AA emissions from Europe and North America (Wild, 2012;

3

Bonfils et al., 2020). The sixth IPCC assessment report (AR6; IPCC 2021) concluded that precipitation would very likely increase over high latitudes and some monsoon regions, while decreasing over parts of the subtropics and tropics, under the SSP2-4.5, SSP3-7.0, and SSP5-8.5 emission scenarios. In terms of zonal averages, a latitudinal redistribution of precipitation, featuring increasing precipitation at high latitudes, and decreasing precipitation at sub-tropical latitudes (Zhang et al., 2007) was attributed in part to anthropogenic forcing. Other examples of attributable human influences on precipitation at the zonal to regional scales include the following: an increase in precipitation at high latitudes in the northern hemisphere (Min et al. 2008; Wan et al. 2015; Knutson and Zeng 2018), over southeastern South America during summertime (Zhang et al. 2016), and the Sahel region since the 1980s (Dong and Sutton 2015). A decrease in precipitation has been attributed to human influence in the Mediterranean region in winter (Hoerling et al. 2012; Christidis and Stott, 2022), the southern and southwest Australia in March−August (Delworth and Zeng, 2014) and the Sahel region from the 1950s to the 1980s (Rotstayn et al., 2002; Held et al. 2005; Undorf et al., 2018). The effects of GHG and AA are also indicated to influence the monsoon flow and precipitation over monsoon regions, North American, West African monsoon, South and South East Asian, East Asian monsoon, South American, Australian, equatorial America and South Africa (Bollasina et al., 2011; Polson et al., 2014; Sanap et al., 2015; Krishnan et al., 2016; Lau and Kim, 2017; Undorf et al., 2018; Ayantika et al., 2021; Douville et al., 2021). And the changes in natural aerosol in response to anthropogenic forcings further influence climate change (Bryant et al., 2007; Carslaw et al., 2010; Zhang et al, 2019, 2021; Kok et al., 2023)

To investigate the precipitation changes in response to internal climate variability and anthropogenic forcings, global climate models (GCMs) based on physics, dynamics, and parameterizations of unresolved physical processes are widely used (Hawkins and Sutton, 2011; Orlowsky and Seneviratne 2013; Dirmeyer et al. 2013; Zhao et al., 2018a, b; Adcroft et al., 2019; Held et al., 2019; Dunne et al., 2020). However, the evaluations of model precipitation simulations suggest that current climate models' ability to reproduce the long-term trends of observed precipitation over land has some shortcomings (Orlowsky and Seneviratne 2013; Zhao et al. 2015b; Knutson and Zeng 2018; Vicente‑ Serrano et al., 2021).

4

The model discrepancies vs. observations are due to various factors, including internal climate variability and the specified historical forcings/model response to forcings for various spatial and temporal scales (Hawkins and Sutton, 2009, 2011; Deser et al., 2012; Rowell, 2012; Knutti and Sedláček, 2013; Dai and Bloecker, 2019), and even to observational uncertainties (Becker et al. 2013).

To build a better understanding of the causes of observed precipitation changes and increase the robustness of climate models, assessments of historical precipitation are essential. They allow for an evaluation of the biases or shortcomings of current climate models compared to historical observations, and of the potential causes of these biases. Previous studies have evaluated the models' performance by comparing various simulated and observed characteristics of precipitation, including spatial patterns and time series of climatologies, anomalies, and trends (van Oldenborgh et al. 2013; Kumar et al. 2013; Zhao et al. 2015b). Other studies have systematically compared the long-term trends of precipitation in the observations and model simulations from several generations of the Coupled Model Intercomparison Project (CMIP) (Meehl et al., 2007; Taylor et al., 2012; Eyring et al., 2016), including trend, spatial patterns and temporal evolution characteristics (Kumar et al. 2013; Ren et al., 2013; Wilcox et al., 2013; Nasrollahi et al. 2015; Zhao et al. 2015a; Knutson and Zeng 2018; Vicente‑Serrano et al., 2021).

Here our focus is on century-scale historical trends in annual-mean precipitation, while we recognize that a large number of potential measures and metrics of model performance are relevant to the issue of confidence in precipitation simulations. Also, to explore possible underlying causes of biases in simulated precipitation trends, we investigate the role of different types of anthropogenic forcings in the historical simulations.

In this study, we analyze the historical land precipitation changes by two coupled global climate models produced by the National Oceanic and Atmospheric Administration's (NOAA) Geophysical Fluid Dynamics Laboratory (GFDL): GFDL's fourth‑ generation coupled physical climate model (CM4; Held et al., 2019) and Earth System Model (ESM4;

Copyright held by author(s). Unauthenticated | Downloaded 06/27/23 06:21 PM UTC

Dunne et al., 2020). CM4 is GFDL's latest atmosphere-ocean coupled climate model and consists of GFDL's AM4.0 atmospheric model (Zhao et al., 2018a, 2018b) and LM4.0 land model (Held et al., 2019) at about 1 degree (~ 100 km) horizontal resolution, 33 vertical levels, and coupled with MOM6 ocean and SIS2 sea ice models (Adcroft et al., 2019) at 0.25 degree (~ 25 km) horizontal resolution (Held et al., 2019). Compared with CM4, ESM4 is built from a common basis of GFDL's AM4.0 and MOM6, but focuses more on chemistry and ecosystem comprehensiveness, with lower ocean model resolution (about 0.5 degree or ~50 km horizontal resolution), but an increased number of chemistry prognostic tracers (21 chemistry tracers in CM4 versus 82 tracers in ESM4), more vertical levels (49), a higher top and increased vertical resolution of the stratosphere, and more advanced land (Elena Shevliakova, 2020) and ocean biogeochemical models (Stock et al., 2020). CM4 and ESM4 have different climate sensitivities. The transient climate sensitivity of ESM4 (1.6 K) is ~20% lower relative to CM4 (2.1 K) and the equilibrium climate sensitivity (ECS) of ESM4 (3.2 K) is 36% lower than that of CM4.0 (5.0 K). Detailed model descriptions and comparisons can be found in Held et al. (2019) and Dunne et al. (2020).

By analyzing the long-term trends of precipitation from CM4 and ESM4 simulations compared to the observations, the model performances can be evaluated as a step toward possibly improving these models in subsequent model development efforts at GFDL. In addition, the sources of trend biases for ESM4/CM4 historical precipitation are explored using forcing subset experiments. Surface temperature trends from observations and model simulations are also compared to further explore the sources of bias in the modeled precipitation and temperature trends.

In summary, the major objectives of this study are to **1)** explore the consistency and discrepancy between the GFDL ESM4/CM4 model simulations and observations of precipitation, including the spatial patterns and temporal evolution, and **2)** investigate the possible roles of certain anthropogenic forcings (e.g., AAs or greenhouse gases) in the modeled biases for long-term precipitation trends, supported by some limited analysis of regional temperature trends.

6

2. Data and Methodology

This section describes the observed and model data used in this study and the data treatment, including data masking and statistical significance tests.

2.1 Observational datasets

This study employs an observed precipitation dataset from the Global Precipitation Climatology Center (GPCC) and a land temperature dataset from Berkeley Earth Surface Temperatures (BEST) project. These datasets are widely used and provide sufficient spatial-temporal coverage for long-term trend analysis (1915–2014) over at least some land regions of the globe. The GPCC V2020 monthly dataset on a 2.5° ×2.5° grid covers the period from 1891 to 2019 (Becker et al. 2013; Schneider et al., 2020); files downloaded June 2021 from https://www.dwd.de/EN/ourservices/gpcc/gpcc.html). The GPCC dataset is maintained by the Deutscher Wetterdienst, German Weather Service under the auspices of the World Meteorological Organization (WMO). The century-scale trend map based on the GPCC data is broadly similar to that obtained using an alternative precipitation dataset (the Climatic Research Unit CRU_ts3.24.01 monthly precipitation dataset on an 0.5º x 0.5º grid; https://crudata.uea.ac.uk/cru/data/hrg/; updated from Harris et al. 2014); see trend comparison in Knutson and Zeng (2018).

While our primary focus is on precipitation trends, in order to analyze the relationship between global/regional precipitation and temperature trends, our study also analyzes the Berkeley Earth land/ocean temperature product (BEST, Rohde et al., 2013a, 2013b; berkeleyearth.org). This land-ocean dataset combines the land analysis (surface air temperature) with an interpolated version of the HadSST sea surface temperature data set. The land-gridded data are available at monthly resolution for 1850-present at a 1° × 1° spatial resolution and are generally available over a greater fraction of global land than the GPCC precipitation data.

2.2 GFDL climate model (ESM4 and CM4) numerical experiments

7

In this study, to assess the models' trends of precipitation and temperature, historical all-forcing simulations (1850–2014) by CM4 (Guo et al., 2018) and ESM4 (Krasting et al., 2018) models are used following the design of the CMIP6 DECK protocol (Eyring et al., 2016). The historical all-forcing CM4 and ESM4 experiments are driven by a comprehensive set of observed anthropogenic and natural forcing agents, including GHGs, AAs, natural aerosols, ozone, volcanic aerosols, solar variations, land-use changes, etc. The all-forcing historical experiments by each model include three ensemble members, which are averaged to reduce the influence of internal variability and obtain an estimate of the forced response.

To further explore the potential drivers of historical regional trends of precipitation and investigate the causes of the potential model bias, we also analyzed forcing subset experiments that used subsets of realistic time-varying historical forcing agents in combination with unchanged preindustrial levels for other forcing agents. The analyzed forcing subset experiments of ESM4 and CM4 include: hist-aer (1 ensemble member; all anthropogenic and natural forcings except historical anthropogenic aerosols are set to preindustrial levels) (ESM4 hist-aer by Horowitz et al., 2018a), hist-GHG (1 ensemble member; only historical well-mixed greenhouse gas concentrations) (ESM4 hist-GHG by Horowitz et al., 2018b), and hist-nat (2 ensemble members; only historical natural forcings from solar variability and volcanic emissions) (CM4 hist-nat by Ploshay et al., 2018; ESM4 hist-nat by Horowitz et al., 2018c). Historical ESM4 and CM4 simulations with observed sea surface temperatures and sea-ice concentration (SIC) from 1870 to 2015 (known as LongAMIP runs, 1 ensemble member) are designed to capture the effects of internal sea surface temperature and sea ice variability on land climate variability. These experiments allow investigation of the potential local and remote ocean SST effects (forced response and natural variability combined) on the land precipitation changes.

Lacking a larger ensemble size for the historical forcing runs, the 530-yr pre-industrial control (piControl) runs from ESM4 and CM4 models are used to test the potential influence of internal climate variability on the model on trends.

2.3. Methods

2.3.1 Data sampling

Due to the uneven spatial distribution of rain gauges in the early decades of the twentieth century and the changing data coverage of GPCC observations with time, our analysis of precipitation starts from the year 1915, as a compromise between providing adequate spatial coverage while attempting to have sufficient observations available at a grid location in the early decades to compute a reasonably well-constrained trend. The model precipitation data are regridded to the GPCC observed grids, and locations and times where GPCC data are not available are set to missing in the model data sets. The aim was to have roughly the same degree of space-time coverage in the observed and modeled datasets, allowing for more "apples to apples" comparisons between the observed and modeled trends. In the trend map analysis, to screen for sufficient data coverage in time for the trend analysis at a particular grid point, the following criteria from Hartmann et al. (2013) and Knutson and Zeng (2018) are used: to be included, time series at a grid point must contain, for the first 10% and the last 10% of the time series, at least 20% data availability, and the entire record must have at least 70% data coverage. In the analysis of spatial averages, the GPCC data availability evolves during the early years, which can introduce or eliminate grid points that can affect the regional-mean climatology. To address its potential influences, the data availability of the GPCC in the first 20 years is used to mask the observational and model datasets, and the regional time series are created by averaging precipitation monthly anomalies (rather than full values) from each unmasked grid point.

The model temperature data are masked according to the data availability of the BEST observations using the same method, and due to superior data coverage for the temperature data, the areas of available data coverage are larger for the temperature time series analyses than for precipitation.

2.3.2 Quantification of internal variability

Previous studies show that internal climate variability can influence trends of precipitation and temperatures in observations and model simulations, especially at decadal-

9

multidecadal and regional scales (Deser et al., 2012; Knutson et al. 2013; Gu et al., 2015; Knutson and Zeng 2018; Dai and Bloecker, 2019; Dai, 2021). Though this paper focuses on the longer-term (century-scale), large-scale changes in precipitation, it is important to quantify the impacts of internal variability for a better understanding of the model-observation differences and model response to external forcings. In this study, the impacts of internal climate variability are quantified in two ways.

First, we compare the spread of individual ensemble members of ESM4 and CM4 historical all-forcing simulations with the model-observation differences. Second, while lacking a large set of ensemble members (only 3 members for each of ESM4 and CM4 all-forcing runs, and single members for the forcing subset runs), the potential influence of internal variability on trends is quantified by using the piControl simulations. From the 530-yr ESM4 and CM4 piControl runs, we sample century-long segments and examine the distribution of trends that arise due to internal variability. The 5th-95th confidence intervals based on these samples are placed around the ensemble-mean trends of the forced simulations and the resulting distribution compared with the observed trend to assess whether the model forced response is consistent with or inconsistent with observations, accounting for internal variability.

3. Results

3.1 Assessment of historical precipitation trends (1915–2014) over land regions

CM4 and ESM4 are shown to have different equilibrium climate sensitivities (5.0 K and 3.2 K) and transient climate responses (2.1 K and 1.6 K) (Dunne et al., 2020; Paulot et al., 2020), and as a result project different climate warming over the 21st century (Fig S1). The different climate sensitivities in ESM4 and CM4 can explain part of the differences between their temperature projections; however, the complex differences in precipitation trends between ESM4 and CM4 suggest the existence of other complicated mechanisms (Fig S1). Here we analyze the historical precipitation trends from long-term model simulations and observations to help us evaluate the models' performance.

10

3.1.1. Precipitation trends maps

To analyze the long-term changes in annual precipitation, the linear regression of the precipitation time series from 1915 to 2014 is used to compare the precipitation changes over the past century between observations and model simulations (Fig.1). As an initial assessment of the statistical significance of the precipitation trends, we used a modified version of the non-parametric Mann–Kendall statistic (Hamed and Rao, 1998; Yue and Wang, 2004). The Mann-Kendall test is a nonparametric test that is used to indicate whether a monotonic trend exists for the century-scale changes in precipitation over each grid by returning the corrected p-values. Based on the Mann-Kendall test, precipitation trend results can be categorized as significant increase or decrease trends (p-value < 0.05) which are denoted by the slashed areas. In the case of experiments with multiple ensemble members, these were combined into an ensemble mean time series before computing the trend and statistical significance tests.
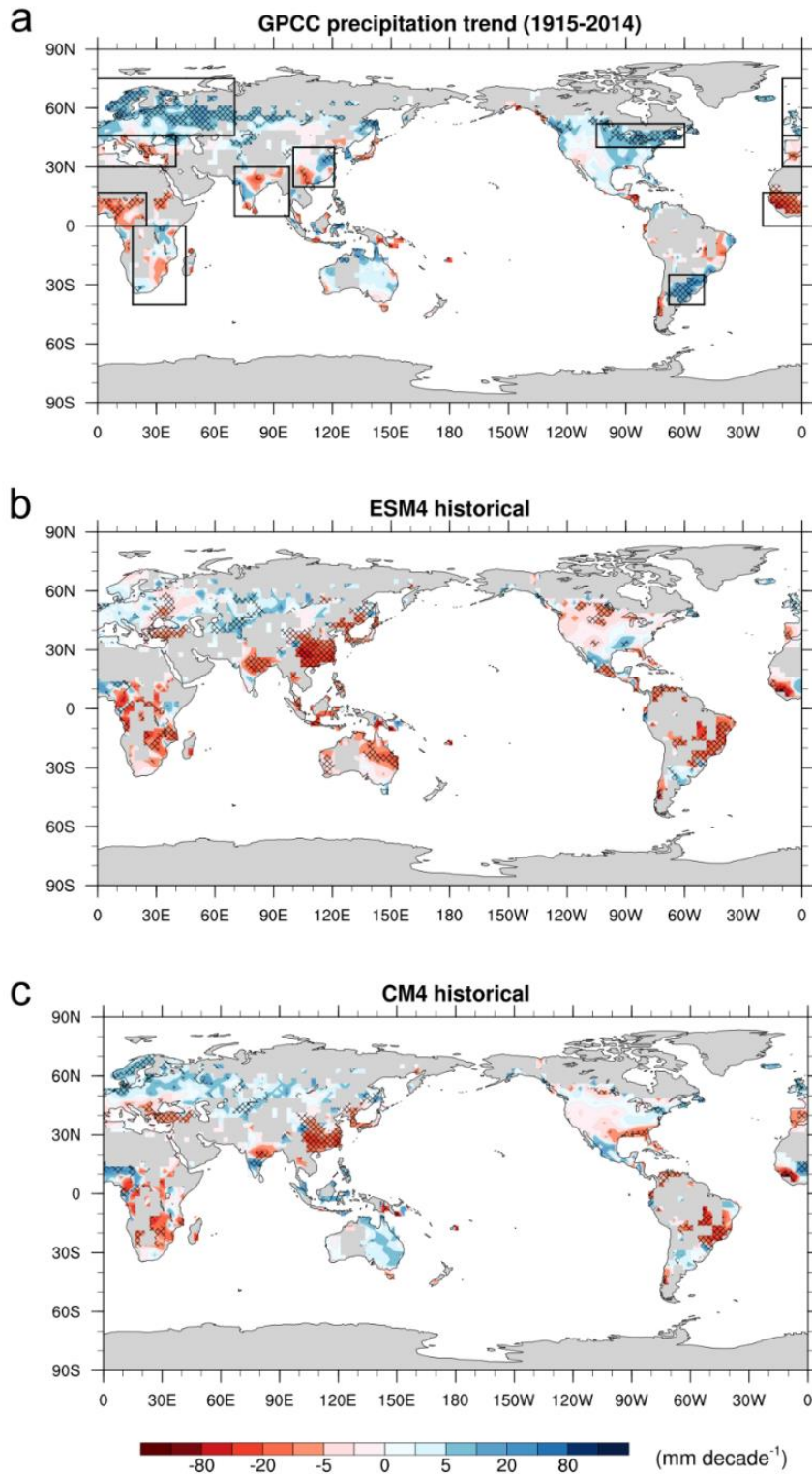
11

Figure 1. Precipitation trends (mm decade⁻¹) over 1915–2014 based on annual GPCC observations (a), and ESM4 (b) and CM4 (c) all-forcing simulations. The precipitation trend uses a p-level of 0.05 for statistical significance, the colored areas with statistically significant positive (blue) and negative (red) precipitation trends are represented by the slashed areas. Grids with missing values are denoted by gray shading. Eight regions selected for the regional analysis are shown in (a).

12

The trend maps in Fig. 1 also indicate the general consistency or differences between annual precipitation changes in observations versus model simulations. These differences between modeled and observed trends are assessed quantitatively for selected regions and zonally averaged bands in Figs. 3 and 6. In the NH, the observed linear trend (1915-2014) map (Fig. 1) shows diverse patterns of precipitation change, but with some prominent coherent features, including significant increasing trends (blue with shading) broadly distributed across the middle to high northern latitudes (~ 45–80° N). The area of significant increases in precipitation broadly covers the whole of Northern Eurasia and Northeastern North America, at least based on the regions with adequate available coverage for trends. At lower latitudes, the observed precipitation trend shows a more heterogeneous pattern, with significant decreases in parts of tropical West Africa, the Mediterranean, northeastern India, and Southwest China, and a significant increase over Eastern China. In the southern hemisphere, the observed precipitation only shows significant increasing trends in small regions of Northern Australia and the La Plata Basin in southern South America.

The CM4 and ESM4 historical all-forcing runs capture many features of the broad general distribution of the observed drying and wetting trends. However, the simulated precipitation trends exhibit a clear bias, with underestimated increasing and unrealistic decreasing trends compared to observations in the extratropical Northern Hemisphere, particularly over regions of North America, East Asia, and the middle to high northern latitudinal band (~15–80° N). The magnitude of the negative biases in the long-term trend of land precipitation is more pronounced in ESM4 than CM4, illustrated by the weaker-than-observed simulated increase with smaller coverage over northern Europe and the relatively stronger decrease simulated over East Asia in ESM4.

Forcing subset runs (hist-aer, GHG, and nat) from ESM4 and CM4 are shown in Fig. 2 to explore the influences of different types of forcing agents on the simulated trends of precipitation. Although the historical simulation (all-forcing) is not a linear combination of the three individual forcing subset runs, the forcing subset runs are analyzed to explore the potential main causes of the simulation biases. The ESM4 and CM4 hist-aer runs show

13

significant decreasing precipitation trends at middle and low latitudes in the NH (~ 0–45° N), especially over the regions of central Europe, East Asia, South Asia, and northern tropical Africa (Figs. 2 a & b). Thus, the model results demonstrate a negative contribution from AA forcing to land precipitation trends in the NH over the last century. In contrast, the linear trends from the ESM4 and CM4 hist-GHG runs show significant increases in land precipitation over most of the observed-data-available regions of the NH (with some exceptions in the Mediterranean region and parts of Central America and central North America) indicating the generally positive contributions from the GHG forcing to the precipitation trends (Fig. 2 c & d). In the natural-forcing-only experiments, the simulated changes in land precipitation tend to be less pronounced than in the hist-GHG and hist-aer experiments in both ESM4 and CM4. In the NH, the negative contribution of AA and positive contribution of GHG-only forcings to the precipitation trends suggest that the models' drying trend bias could be due to some combination of overestimated aerosol negative effects and underestimated GHG positive effects.

Besides the external forcings (GHG and AA), internal climate variability is also indicated to influence precipitation changes (Deser et al., 2012; Rowell, 2012; Knutti and Sedláček, 2013; Knutson and Zeng 2018; Dai and Bloecker, 2019). The maps of land precipitation trends by ESM4 and CM4 individual all-forcing ensemble members (r1, r2, and r3) are given in Fig. S2. While there are no obvious differences in most of the NH among ESM4 and CM4 ensemble members, ESM4 shows some spread between individual ensemble runs over the regions of northern Europe and the Mediterranean. However, the precipitation tendencies by individual ESM4 ensemble runs are all substantially lower than the observed trend over Europe. This result suggests that the internal variability influences regional precipitation changes, but the differences between observations, ESM4, and CM4 simulations are likely dominated by the external forcings and related model responses.
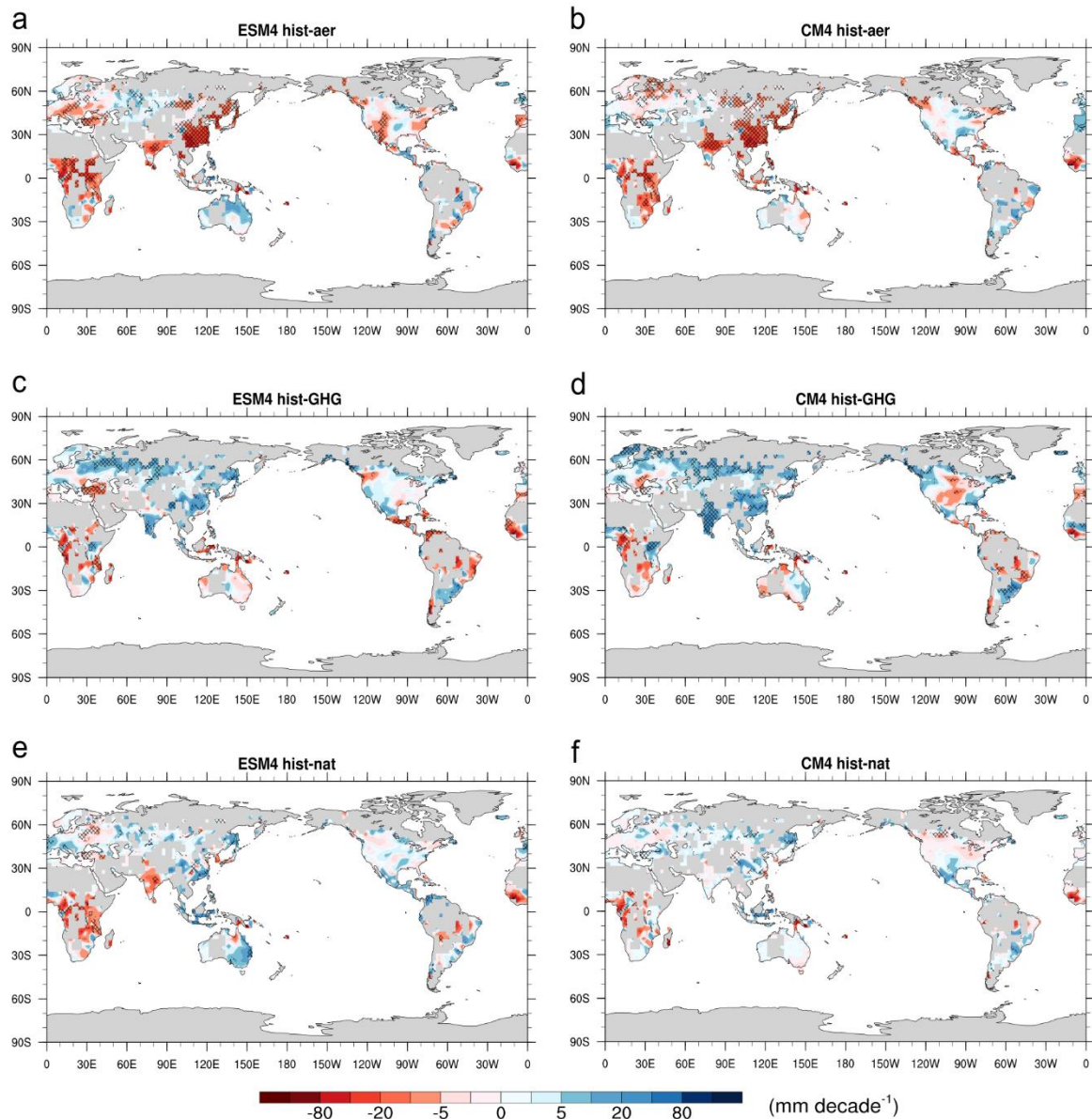
Figure 2. As in Fig. 1, but for assessments of precipitation trends by model forcing-subset runs, ESM4-aer (a, anthropogenic aerosol only run), GHG (c, greenhouse gases only run), nat (e, natural forcing only run), and CM4-aer (b), GHG (d), and nat (f).

3.1.2. Land precipitation trends over latitudinal bands

To further quantitatively assess the differences in the behavior of the two models and their differences with observations, zonal-mean trends and time series of land precipitation are analyzed for different latitudinal bands (Figs. 3 and 4). The anomalies were calculated as the deviation from the 30-yr mean monthly precipitation climatology (using the period of 1970-1999, with the best data coverage, to construct the climatology). Using anomalies helps

15

to reduce problems when time series values for individual grid points are missing for some time periods and thus cannot be used in creating a spatial average for certain periods.

Fig. 3 shows the 100-yr trends of available land precipitation anomalies. Over the global (60° S–80° N) and NH (0–80° N) land domains, there is a slight (nonsignificant) increasing trends in the observed precipitation but significant decreases in the model all-forcing runs (Fig. 3 a & b). In the tropics and NH extratropics, the zonal mean annual precipitation trends in observations and model simulations show various degrees of consistency for different latitudinal bands (Fig. 3 c–e). In the tropical region (15° S–15° N), Fig. 3 shows no significant differences between the area-averaged observed and model trends of precipitation anomaly. The discrepancy between the average trends in observations and the model historical simulations is more significant in extratropical NH (Fig. 3 d–e). For 15°–45° N, no significant changing trend was indicated for the GPCC observations, however, both ESM4 and CM4 simulated significant decreasing trends of precipitation. For 45°–80° N, both ESM4 and CM4 all-forcing runs significantly underestimate the long-term increasing trend in the observations.

To assess whether the model-observation difference could be caused by internal climate variability or model responses to external forcings, the spread among ESM4 and CM4 ensemble members (r1, r2, and r3) is compared with the discrepancy from the observed precipitation trend. The r1–r3 results show little spread, suggesting that internal variability likely cannot explain the difference between the observations and the all-forcing simulation. Additionally, the observed trend is located outside of the 5th–95th confidence region of modeled all-forcing ensemble precipitation trends (except for ESM4 for 15° S–15° N). These results demonstrate that the substantial differences in the long-term precipitation trend between the observations and all-forcing simulations in the extratropical NH are not due to internal variability, but likely have a substantial contribution from the models' response to external forcings. In other words, the modeled trends are generally shown to be significantly different from observations in all of the regions (outside of 15° S–15° N), even accounting for the influence of internal variability.
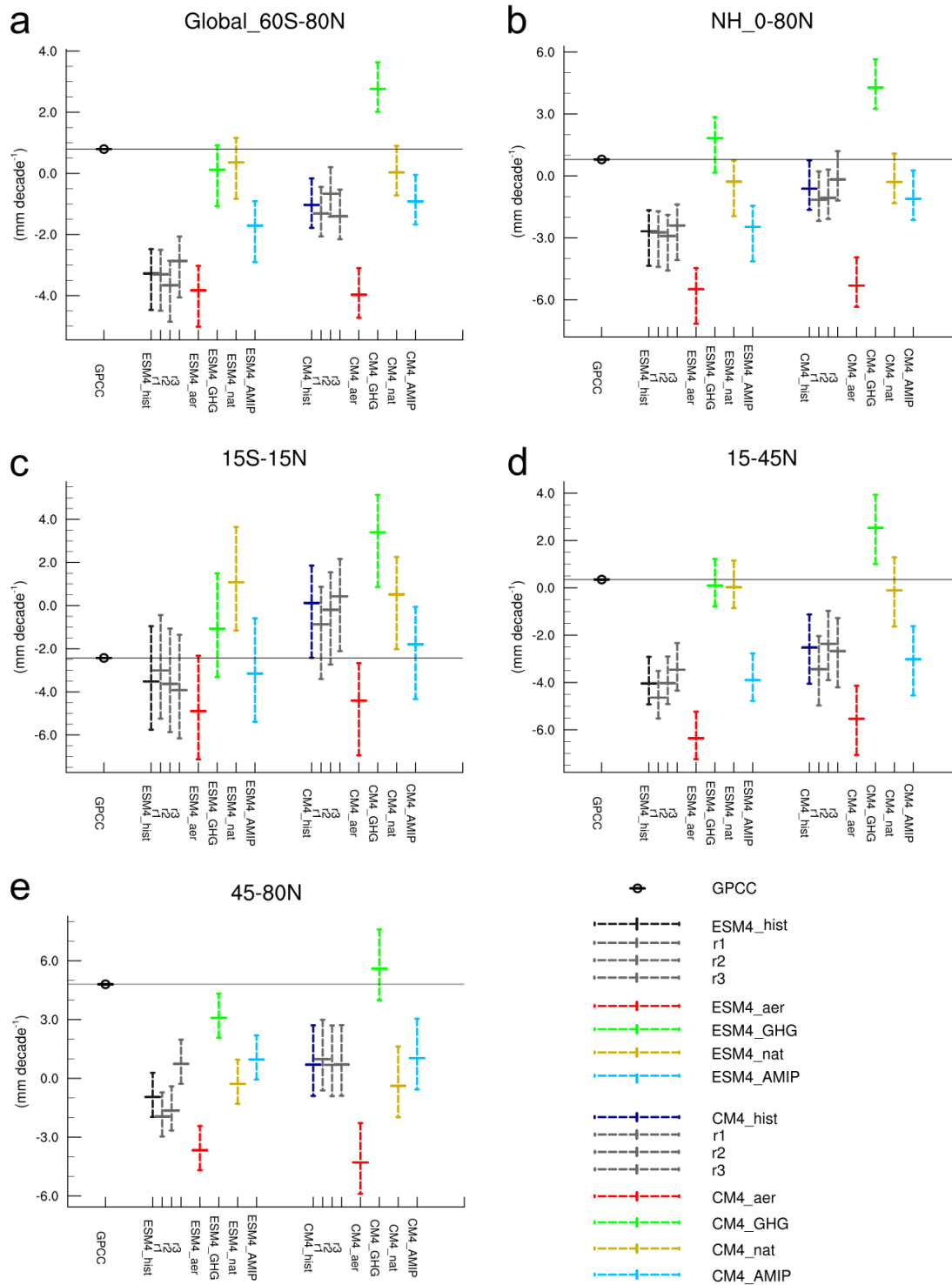
16

Figure 3. Global (a), NH (b), and zonal-mean (c–e) trends of land precipitation anomaly (1915–2014; mm decade^{-1}) from the GPCC observation, ESM4/CM4 all-forcing ensemble mean (hist) and members (r1, r2, and r3), forcing subset (aer, GHG, and nat), and long-AMIP (AMIP) simulations. The linear trend and distributions (5th–95th percentiles based on the piControl runs) for individual model runs are shown by short vertical line segments and colored bars. The observed (GPCC) precipitation trends are denoted by the large black dots and horizontal lines.

The zonal-mean precipitation trends from the historical all-forcing and forcing-subset runs in Fig. 3 show the overall positive and negative contributions from GHG (green bars) and AA (red bars) forcings to the simulated precipitation trends, respectively. The comparison of the precipitation trends between the ESM4 and CM4 forcing subset runs shows that the ESM4 GHG-only forcing contributes a weaker increase, leading to a more significant underestimation than in the CM4 GHG-only simulation. It is also notable that the latitudinally averaged results from the LongAMIP runs (blue bars) for 15°–45° N and 45°–80° N show roughly the same significant differences with observed long-term precipitation trends for both ESM4 and CM4 as was found for the all-forcing runs. This result suggests that even specifying the SSTs and sea ice changes over the past century, along with specified changes in climate forcing agents, does not lead to an adequate simulation of the historical trends in the northern mid to high latitudes.

To explore the potential mechanisms that may drive the precipitation evolutions at decadal time-scales in response to changes in forcings and further elucidate model biases, the 10-yr running mean zonal-averaged time series of precipitation anomalies are shown in Fig. 4. Over the tropical land (15°N-15°S), the GPCC observations show no clear trends until 1960, decreasing precipitation over 1960-1990, and increasing precipitation from 1990 to 2014. This temporal variation of the observed tropical precipitation trends is fairly well depicted by the ESM4 and CM4 all-forcing runs (Fig. 4 c). However, the difference between the model simulations and the observations increases with latitude, as shown in panels d, e. For the latitude band 15°–45° N (Fig. 4 d), observed precipitation shows a relatively little trend over the 100-yr period. In contrast, a clear decline in precipitation from the 1930s on can be seen in the ESM4 and CM4 all-forcing and aerosol-only runs. The results indicate that the AA forcing drives a long-term decreasing trend of simulated precipitation in this latitudinal band. At higher latitudes (45°–80° N; Fig. 4e), the observed precipitation predominantly increases since the mid-1940s. Conversely, the ESM4 and CM4 all-forcing runs simulate clear decreases between the 1950s and 1970s, leading to a marked departure from the observed time series. Although the models simulate increases after the 1980s that are stronger than the observations, the unrealistic decrease from the 1950s to the 1970s leads

to a clear underestimation of the observed long-term increasing precipitation trend. The multi-decadal decrease of precipitation (45°–80° N) in the all-forcing experiments is well-captured in the AA-only runs, suggesting that an overestimation of aerosol forcing and/or response to this forcing is a critical factor in producing the dry trend bias of ESM4/CM4 historical runs precipitation in the middle–high latitudes.
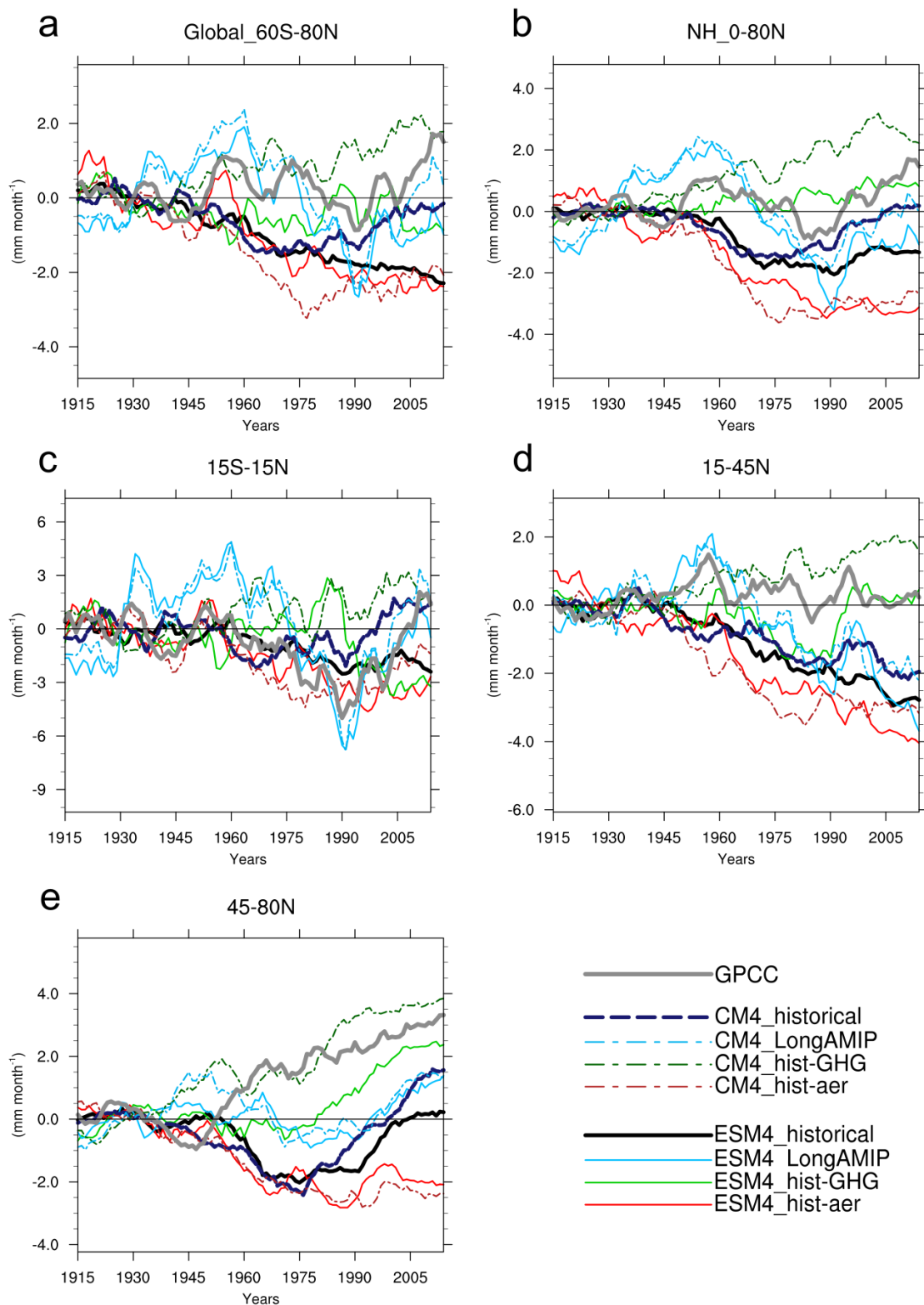
Figure 4. Zonal mean time series of land precipitation anomalies (1915–2014) for different latitudinal bands in the Northern hemisphere from the GPCC observations, ESM4/CM4 historical all-forcing ensemble mean, aerosol, GHG, and long-AMIP runs with specified SSTs (see legends). The 10-yr running mean observations and model anomaly time series shown are calculated by subtracting the mean value averaged over the first 30 years (1915–1945).

Besides the model-observation differences, the linear trends and temporal evolutions (Figs. 3 and 4) show statistically significant differences between the all-forcing simulations by ESM4 and CM4. The evident differences between the GHG-only precipitation simulations along with the similar trends in the aerosol-only runs suggest that the differences between ESM4 and CM4 historical precipitation are partially due to differences in the GHG responses. However, this difference could also be due to other factors, including different natural aerosol responses, other biospheric feedbacks, etc.

The results for both models show no clear long-term trends in their natural forcing-only runs, which suggests that the statistically significant trends of observed historical land precipitation are not likely to have been caused by the natural forcing. Thus, the analysis above mainly focused on the effects of GHG and aerosol forcings.

The relationship between the modeled response to anthropogenic forcings and the dry bias of model precipitation in the extratropical NH is further illustrated in Fig. 5, where we compute a time-evolving model minus observation difference estimate for precipitation, based on anomalies from a 1915-1945 baseline. This difference estimate is not meant to assess the bias in mean precipitation amounts over the period, but rather to highlight issues with how the precipitation anomalies are changing over time during the all-forcing runs compared to observations. For the band 15°–45° N, the zonal mean ESM4 and CM4 historical land precipitation differences vs. observations increase in magnitude as the all-forcing runs have an increasingly negative tendency of precipitation, compared to observations, over 1945-1970. This time evolution is similar to the simulated precipitation changes for the AA-only simulation, suggesting that the overestimation of AA forcing or the aerosol-related model response is the critical driver of the models' long-term low trend biases (Fig. 5 d). A similar feature is also demonstrated at higher latitudes (45°–80° N; Fig. 5e): a strong increase in the magnitude of the modeled precipitation differences vs. observations occurs from 1945-1970, followed by a period of relatively unchanging differences from 1970-2014. In this case, the aerosol-only runs show a similar negative tendency over 1945-1970, though not as strongly as shown in the historical run differences from observations.
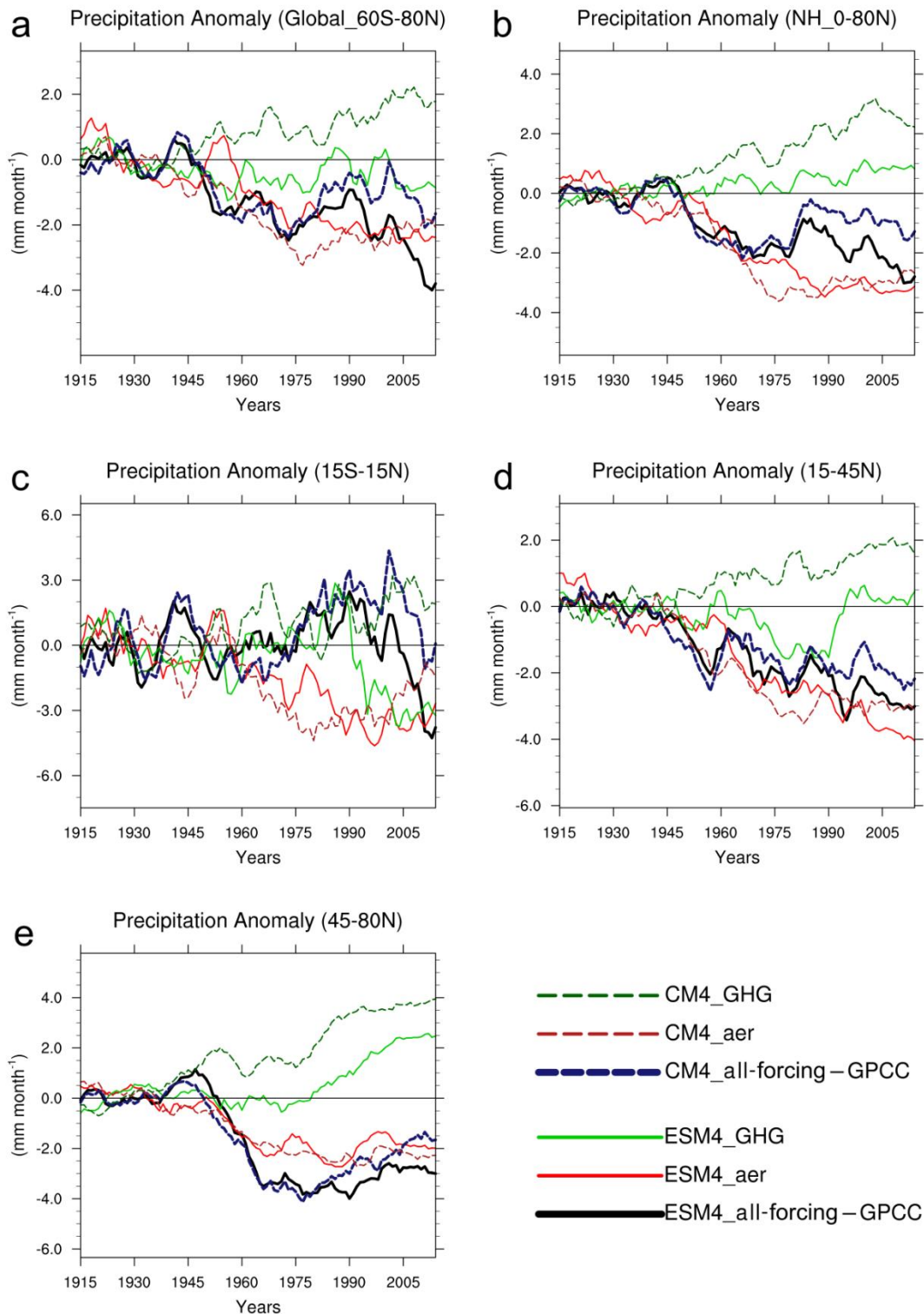
21

Figure 5. Zonal mean time series of all-forcing precipitation change differences vs. observations (computed as all-forcing model precipitation minus observations, based on anomalies from a 1915-1945 reference period). The difference vs. observations for the all-forcing runs is compared with the precipitation differences vs. observations from the greenhouse gas-only and AA-only experiments for different latitudinal bands in the Northern hemisphere (see legends).

3.1.3. Land precipitation responses for selected regions

As a latitudinal band generally spans multiple continents with regions of diverse climate zones and potential mechanisms of precipitation changes, the zonal means may obscure important characteristics of precipitation trends over different regions within the latitude bands. Thus, eight regions (denoted by black boxes in Fig. 1 a) are selected to further assess the regional long-term precipitation trends in observations and model simulations (Fig. 6 and Fig. S3). The results show that the ESM4 and CM4 all-forcing simulations and observed trends (1915-2014) are statistically consistent (Fig. S3) over some regions such as South Asia (Fig. S3 a), and the Mediterranean (c). Here we choose the regions with the most significant model-observation differences in order to investigate the modeled precipitation trend biases and their potential causes at the regional scale.
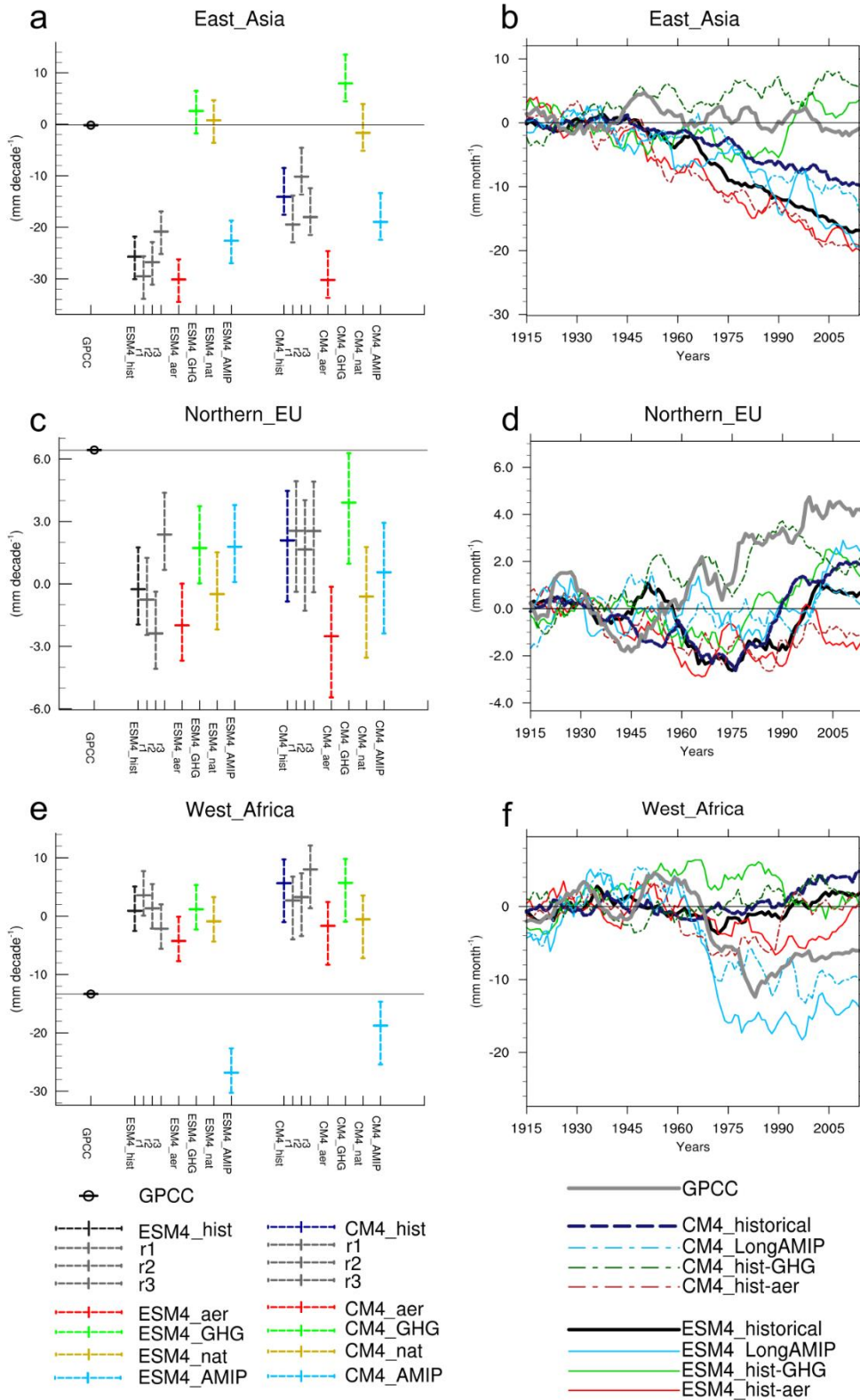
23

Figure 6. As in Figs. 3 and 4, but for the linear trends and time series of precipitation anomaly (with 5th - 95th range) in the observations and model simulations averaged in the regions of East Asia (a, b), Northern EU (c, d), and West Africa (e, f) as shown in Fig.1 a.

Over East Asia, increases and decreases in precipitation are observed over parts of the region (Fig. 1 a) while the regional averaged trend shows no significant change (Figs. 6a, b). Both ESM4 and CM4 all-forcing runs simulate a strong and homogeneously distributed decrease in precipitation (Fig. 1 b, c), leading to the statistically significant negative bias in precipitation trends in this region. In Northern Europe, ESM4 and CM4 historical simulations significantly underestimate the observed increasing trend of precipitation in the past century (Fig. 6 c, d) associated with the unrealistically large simulated precipitation declines in this region in model all-forcing runs from 1950 to 1975.

In the West Africa region (Fig. 6e, f) the ESM4 and CM4 historical runs failed to depict the observed very pronounced decrease in annual-mean precipitation over 1960–1980, associated with the Sahel drought (Held et al. 2005). However, experiments using prescribed SST and sea ice (ESM4 and CM4 long-AMIP runs) indicate that these models can broadly reproduce observed trends and temporal variation of precipitation in West Africa (with a noticeably stronger than observed decline over 1960-1980 simulated in ESM4). The results suggest that the multidecadal variability of SST (which may include forced SST signals not captured by the model as well as multidecadal internal climate variability) may be responsible for a significant amount of the observed multidecadal precipitation variability in the West Africa region.

In the IPCC AR6 report, the Sahel drought during 1960–1980 was inferred to be related to sulphate aerosol emissions, which caused key inter-hemispheric SST anomalies and related regional precipitation changes (Douville et al. 2021). However, in the GFDL models and other CMIP6 models, the anthropogenic forcings (both AA and GHG) show very limited influences on the changes in monsoon precipitation over West Africa (Douville et al. 2021), indicating some inconsistencies in the current generation of GCMs/ESMs for the inferred mechanism of this important precipitation/drought variability feature.

3.1.4. Discussion of the Land precipitation trends and model bias

From the above long-term analysis of precipitation over land, the comparisons of models

25

and observations suggest a particularly pronounced dry bias of the century-scale trends in the all-forcing simulations in the middle and high latitudes in the NH, especially over the regions of northern Europe and East Asia. At the century scale, the spread among the ensemble members (Figs. 6, S2 and S4) and the 5–95% confidence range (Figs. 3 and 6) suggest that a combination of errors in external forcings and related modeled responses are major factors producing discrepancies between modeled and observed precipitation and that the discrepancies are likely not just due to internal variability, at least based on the potential influence of internal variability as estimated by the models. However, for the more recent 50-year period (1965–2014) the models do not exhibit prominent dry trend biases over the NH land regions (Figs. S3 and S5). Rather, the models' simulations over the recent period show a better consistency of all-forcing trends with the observations at mid-high latitude (45°–80° N) than that at the century-scale (Figs. S5 a–c and S6). These differences in model's abilities to reproduce observed precipitation trends over different periods (1915–2014 and 1965–2014) are possibly caused by many factors. Previous studies indicate that shorter-term trends can be more influenced by internal climate variability, which is also shown by the spread between ensemble members and the 95% range of the 50-yr trend (Figs. S6 and S7).

In this study, it is notable that the trends over the period 1965-2014 do not include the full influence of the marked (unrealistic) decrease in precipitation simulated between ~1950–1980, which seems to be related to aerosol forcing in the models. The precipitation trends at different time scales show that, over northern Europe, analyses of short-term (e.g., 50-year, 1965-2014) model simulated trends do not show the significant dry bias as was found for the century-scale (1915-2014) trends, meanwhile the significant dry bias over East Asia still exists for the short-term period. This difference could be related to the regional divergence of aerosol evolutions, i.e., the aerosol loading decreased since the most polluted era (~1970) over Europe but kept increasing over Asia in the post-1980 period.

A correlation between the aerosol effects and precipitation changes was previously indicated by a series of studies mainly through two major pathways: by influencing the radiation and cloud microphysical properties (Douville et al. 2021). Aerosols are shown to

scatter and absorb solar radiation which reduces surface evaporation and precipitation subsequently (Ming et al., 2010; Douville et al. 2021). Due to the dimming caused by AA emissions from Europe and North America, the NH precipitation is indicated to decrease over ~1950–1980 and increase thereafter following the improved air quality (Wild, 2012; Bonfils et al., 2020; Douville et al. 2021). The aerosol cooling in the NH leads to the southward shift in the tropical rain belt (Allen et al., 2014, 2015; Brönnimann et al., 2015) and the weakened monsoon flow and precipitation (Krishnan et al., 2016; Lau and Kim, 2017; Lin et al., 2018; Undorf et al., 2018; Ayantika et al., 2021). Research also shows that the increase in Asian aerosol leads to substantial changes in Asia Monsoon rainfall and extreme precipitation (Guo et al., 2013; Li et al., 2016; Lin et al., 2018; Wilcox et al., 2020), but the effects of Asia aerosol on long-term precipitation trends are relatively less studied. In this study, the temporal-spatial properties of the model-observation differences suggest that the dry bias in ESM4 and CM4 historical precipitation simulation could be due to the overestimated aerosol forcing or related model responses.

Multidecadal precipitation variability over tropical land (15°S–15°N and the tropical west Africa region), as seen in observations (Figs. 4c, 6f), can be produced to some extent in the LongAMIP simulations that include observed SST influences, as well as the same greenhouse gas concentrations and aerosol emissions as the all-forcing simulations. This can be seen by comparing model historical (all-forcing) and LongAMIP simulations in Figs. 4c and 6f. The ability of LongAMIP runs to simulate multidecadal variations of observed tropical land precipitation was also examined in a previous study (Liu and Allen, 2013, their Fig. 3). The modeled observed SST influences (e.g., difference between historical (all-forcing) ensemble mean and the LongAMIP runs) can include two influences: i) effects of observed internal variability (which in the all-forcing model ensemble is of random phase and partially filtered out by ensemble averaging) and ii) discrepancies between the climate response to forcing in the model vs. the real world (which can be partly due to errors in forcings or missing processes in the models). Supplemental Fig. S8c shows a comparison between the all-forcing runs precipitation discrepancy (all-forcing minus GPCC) vs. the discrepancy including observed SST in the models (LongAMIP minus GPCC). When

averaged over 15°S–15°N, discrepancies between observed precipitation and either the ESM4/CM4 all-forcing or the LongAMIP simulations are generally similar in magnitude. The results for tropical west Africa in 6f suggest that observed SST multidecadal variations played a critical role in the observed multidecadal precipitation variability over tropical west African land regions. However, the extent to which the differences between modeled and observed precipitation variations in this region are due to under-simulated internal variability influences or a combination of errors in forcing and related responses is still uncertain. Errors in forced response may even include missing forcings or incorrectly modeled processes that are not yet incorporated into the models. As one example, in the Sahel and neighboring regions, irrigation activities in the Middle East and South Asia could have a remote influence on precipitation sensitivity (Zeng et al., 2022).

For the higher latitudes (15–45°N and 45–80°N), the time series in Fig. 4 demonstrate that observed SST influences cannot account for the differences in precipitation between observations and model historical simulations since the 1960s in these models. This suggests that the model precipitation trend bias in the extratropical Northern Hemisphere is primarily dominated by anthropogenic forcings and related model responses.

3.2 Assessment of near-surface temperature over land regions

While the primary focus of this study is on precipitation trends, we also analyze near-surface temperature (T_s) trends, since, as part of the hydrological and energy cycle, precipitation is closely related to temperature through various physical processes, such as the Clausius–Clapeyron (CC) relationship, latent heat transfer, moisture transport, etc. (Held and Soden, 2006; IPCC 2014). Previous studies suggest the response to T_s change as a critical factor in the precipitation change mechanism (Andrews et al., 2010). The changes in the NH land precipitation are indicated to be related to the aerosol-cooling by AA emissions from Europe and Northern America (Allen et al., 2015; Brönnimann et al., 2015; Douville et al. 2021).

Here, we analyze T_s as an intermediate factor between precipitation and external

28

forcings, to investigate the mechanisms of the anthropogenic influences on land precipitation trends and the possible causes of the model precipitation trend biases.

Maps of century-scale T_s trends (Fig. 7) show that over 1915-2014, the observed temperature (BEST) shows a statistically significant warming tendency over almost all land regions covered by the dataset, with the strongest increases found at ~40°–60° N. Compared to the observation, the CM4 and ESM4 model all-forcing runs are shown to underestimate the long-term trends of T_s over land (Fig. 7 b & c). The models simulate weaker warming over middle-high latitudes (40°–60° N) and a regional cooling tendency — in contrast to the observed warming — over parts of East Asia. The spread among individual ensemble simulations and the 5th–95th confidence intervals of modeled T_s suggesting the observation-model differences at each latitude band are not dominated by internal variability (Fig. S10).

It is worth noting that the spatial distribution of the underestimated temperature increase in the models is qualitatively consistent with major features of the low biases of the model precipitation trends (Figs. 1 v.s. 7), with smaller-than-observed regional wetting in northern mid- to high latitudes going with smaller-than-observed warming in those regions.

Compared to the all-forcing simulations, the LongAMIP runs simulate improved long-term trends of T_s, particularly for ESM4 (Fig. 7 vs. Fig. S9). However, negative bias areas persist in both the CM4 and ESM4 LongAMIP runs, demonstrating that the model T_s bias cannot be fully reconciled by specifying the SST internal variability. These biases in the LongAMIP runs could be attributable to the local aerosol forcing and the model responses to aerosol changes over land in the LongAMIP runs, including possible deficiencies in direct and indirect effects of aerosol, land-atmosphere feedbacks, and other missing or poorly modeled forcings or processes in the models.
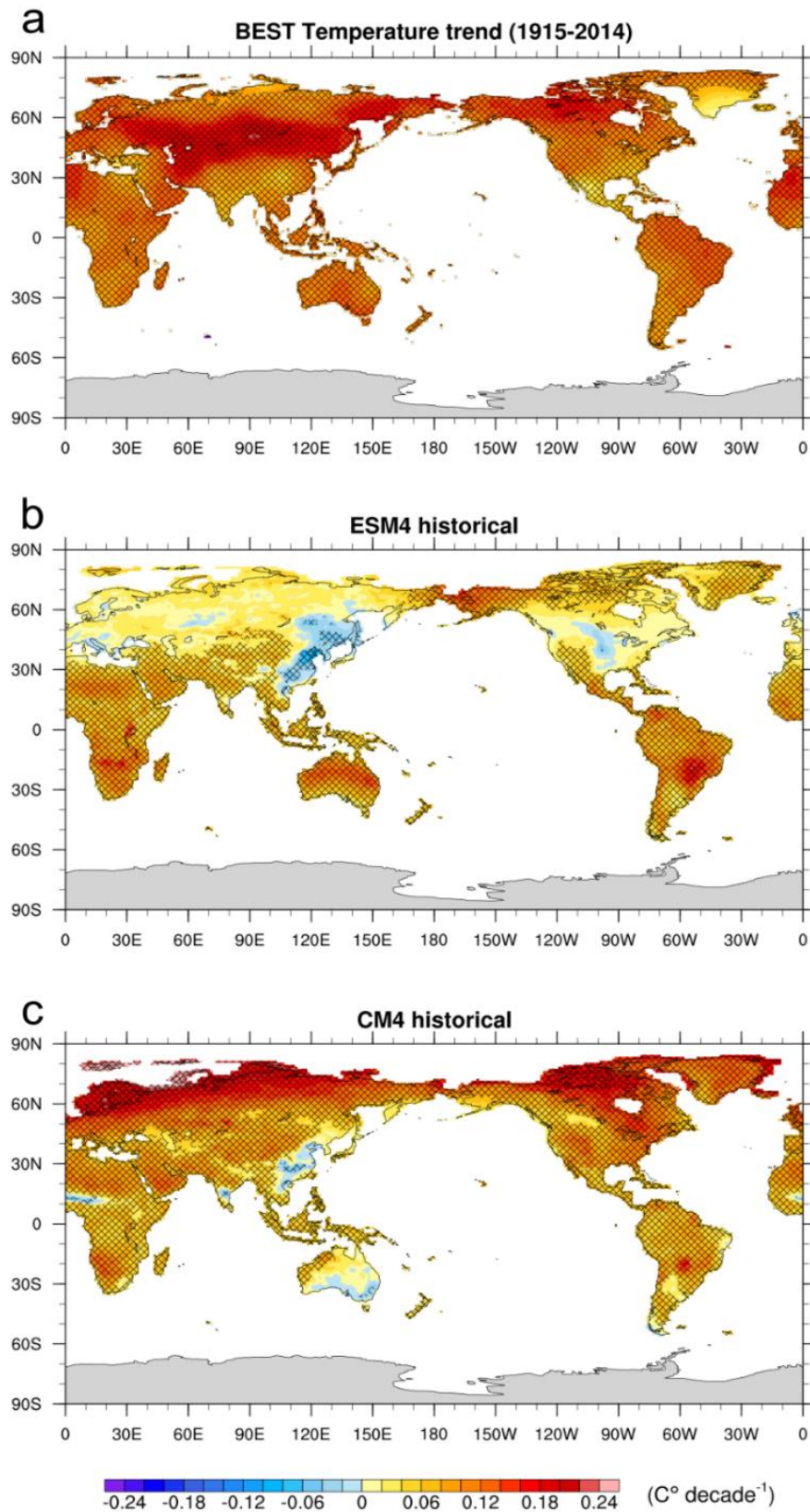
29

Figure 7. Linear-trend maps of near-surface temperature over land grids based on the BEST observations (a), ESM4 (b), and CM4 (c) all-forcing simulations over the period 1915–2014.

Besides the model-observation difference, the comparison between the ESM4 and CM4 all-forcing runs also shows clear differences in the 100-yr trend of T_s. Compared with the rather limited warming in the NH high latitudes by ESM4, the CM4 all-forcing ensemble mean depicts a stronger increase in temperature (Fig. 7 b vs. c). The long-term trends of T_s by the forcing subset experiments (Fig. 8) show that ESM4 and CM4 simulate similar responses of temperature to AA (Fig. 8 a vs. b) and natural forcings (e vs. f). Meanwhile, the CM4 GHG-only run simulates a warming trend that is much stronger than that in the ESM4 GHG run at ~45°–80° N in the NH (c vs. d). The results indicate that the difference between the long-term trends of T_s in the two models is primarily caused by different responses to the GHG-forcing (Fig. 8 c vs. d).

Besides the significant difference between ESM4 and CM4 ensemble mean T_s trends, which is related to the GHG effects, the comparison (Fig. S10) also shows some noticeable spread among individual ESM4 and CM4 ensemble members (r1, r2, and r3), respectively. The result demonstrates that the difference between the two models could be influenced by both internal variability and the response to external forcings.
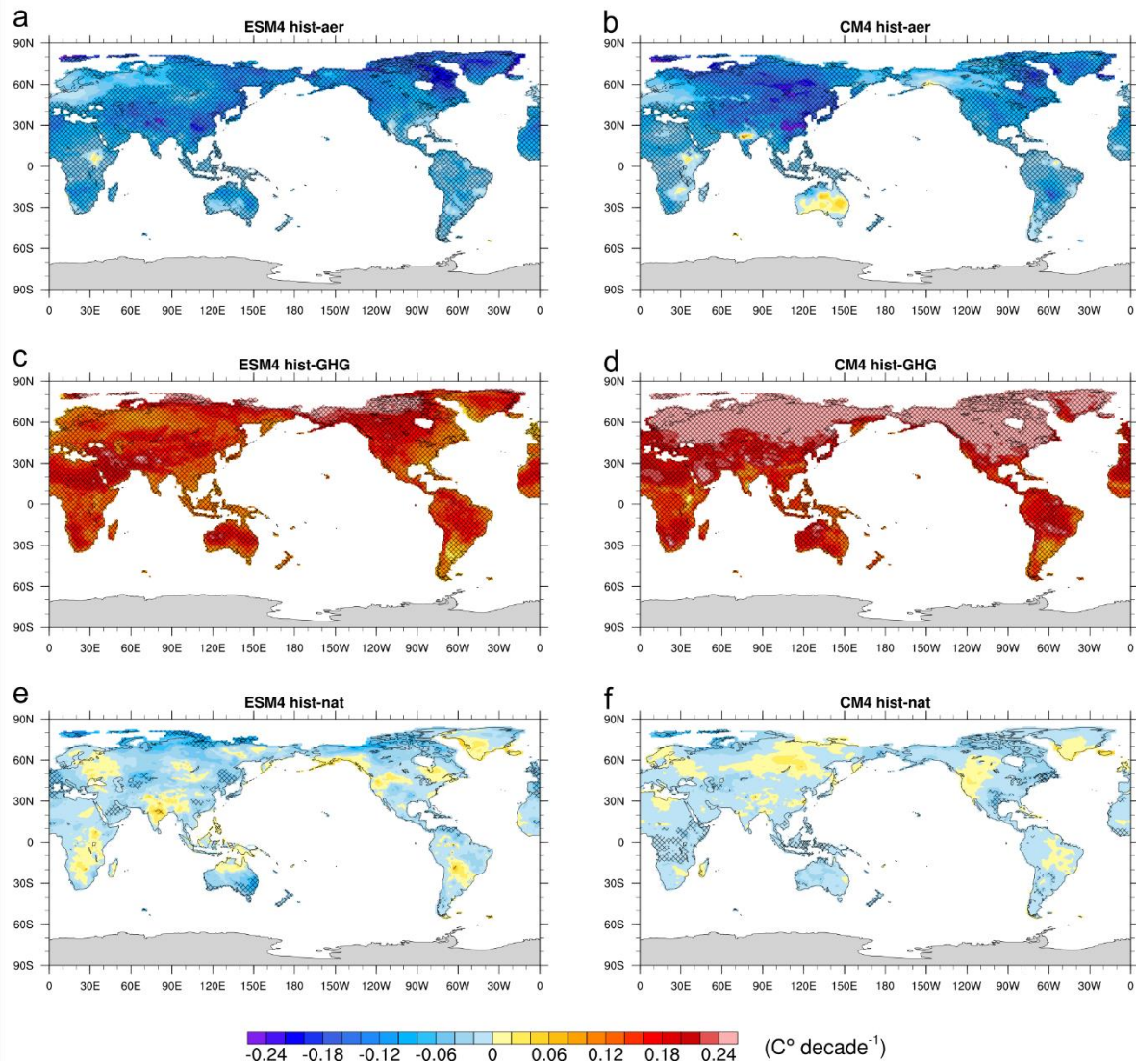
31

Figure 8. Linear-trend maps of near-surface temperature (1915–2014) over the land grids in the ESM4 and CM4 historical aerosol-only (a, b), GHG-only (c, d), and natural forcing-only (e, f) simulations.

The temporal evolutions of zonally averaged T_s in the ESM4 and CM4 all-forcing and forcing subset runs are shown in Fig. 9. The observations show slow warming before 1960, a cooling until ~1970 (except in the tropical region) followed by a rapid increase in recent years. Compared to the observations, the ESM4 and CM4 all-forcing runs simulate a more significant cooling (~1950–1980) followed by a rebound of temperatures. After ~1980, ESM4 and CM4 simulate rates of T_s increase that are similar to or even stronger than the observations in the extratropical NH. The results demonstrate that the underestimation of the long-term T_s trends by the all-forcing runs is primarily resulting from the pronounced decrease in model T_s between ~1950–1980 compared to a more modest decrease in

32

observations. The GHG-forcing warming and the stabilized natural-forcing T_s indicate that aerosol forcing drives NH cooling over ~1950–1980. The roles of AA in the anomalous cooling (or "pothole" cooling) over this period are also indicated by recent studies, and it is notable that an overly strong aerosol cooling commonly exists in the CMIP6 models (Sellar et al., 2019; Dittus et al., 2020; Zhang et al., 2021).

The comparison between ESM4 and CM4 forcing subset runs shows similar T_s evolutions in the AA and natural forcing-only runs, again suggesting that the different responses to GHG forcings is a critical factor in causing the difference between the ESM4 and CM4 all-forcing T_s evolution in the extratropical regions.
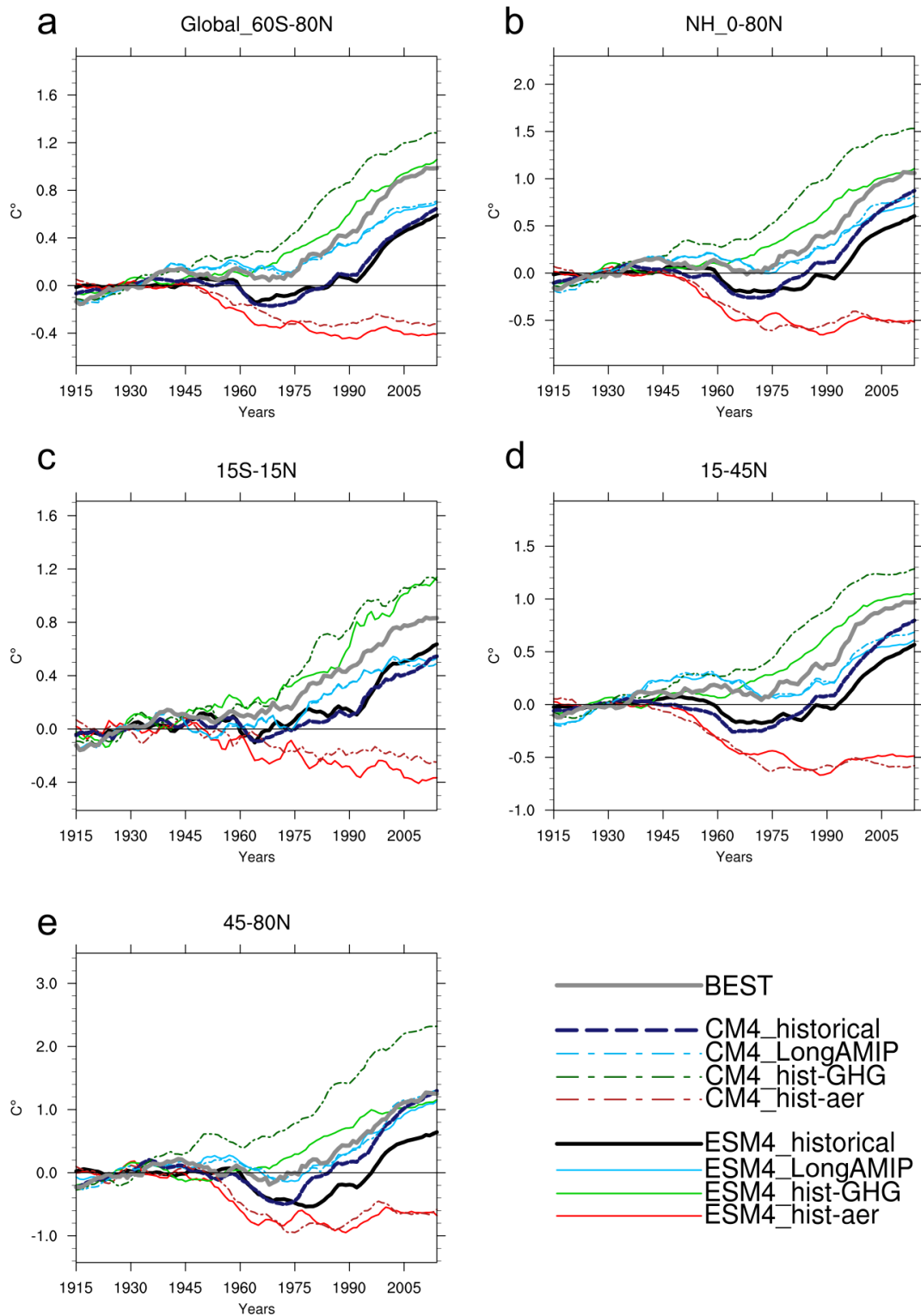
33

Figure 9. Zonal mean near-surface temperature anomaly time series over all land grids (1915–2014) from BEST observations and ESM4/CM4 simulations. The anomalies shown are derived by subtracting the time mean over 1915-1945 from each time series.

By analyzing the long-term trends and temporal evolution, we can investigate the

relationship between the changes in precipitation and temperature. The maps of the long-term linear trend show the consistency between the spatial distributions of the underestimated temperature trends and the low biases of precipitation trends in the model historical simulations in the NH, especially over northern Eurasia and East Asia (Figs. 1 v.s. 7). The time series also show similar features for the model all-forcing temperature and precipitation: the overestimated sharp decrease between ~1950–1980 leads to the model simulations' departure from the observed trends and thus to the underestimation of the 100-yr trends in the models in the mid-high latitudes (Figs. 4 v.s. 9).

As discussed above, the difference in the long-term temperature trend between the observations and model simulations is related to the overestimated model cooling between ~1950–1980, which is predominantly driven by the aerosol forcing (Fig. 9). Thus, the overestimation of aerosol forcing and related model responses is one of the main causes of the low bias in the century-scale trends of modeled historical precipitation. In addition, a comparison of model temperature and precipitation time series suggests that an underestimated GHG response in the models (especially ESM4) could be another important influencing factor.

Results for particular regions (Fig. 6 and Fig. S11) indicate that the areas with the most significant dry bias or underestimated moistening bias of model historical precipitation trends (East Asia, northern Europe, and the northeastern US), are also where the model all-forcing temperatures show a period of decrease (~1950–1980). However, this coherent relationship between temperature and precipitation trend biases cannot be seen clearly in other small regions, which could be due to the stronger influence of internal variability at smaller regional scales.

4. Discussion and conclusions

This study provides an assessment of century-scale (1915–2014) land precipitation trends by comparing observations and simulations by two GFDL coupled climate models--ESM4 and CM4. Near-surface temperature trends are also examined to provide context and to

35

further investigate the possible contributions of various anthropogenic and natural forcings to the modeled precipitation and temperature trend biases.

In the NH, the observed annual land precipitation (GPCC) data shows significant increasing trends in a coherent signal distributed across the mid-high latitudes (45–80° N), with a more heterogeneous pattern of increases and decreases in the middle latitudes (15–45° N). There are significant decreases in parts of West Africa, the Mediterranean, northeastern India, and Southwest China, and a significant increase in Eastern China. Despite some general consistency of spatial patterns between the observations and the model simulations (e.g., for most areas of increases or decreases), the analysis demonstrates a statistically significant dry bias or underestimated moistening bias in the century-scale ESM4 and CM4 historical all-forcing precipitation trends over extratropical land regions with adequate data for trend analysis (15°–45° N and 45°–80° N), particularly over East Asia and northern Eurasia. The zonally averaged time-series show that these century-scale trend differences arise particularly due to discrepancies between the observations and model all-forcing precipitation in the mid-high latitude NH since ~1950. These biases in the models' historical precipitation simulations indicate the limitations of the model's ability to reproduce the historical trends of land precipitation and could imply uncertainties in projections of future land precipitation changes in several regions.

To understand the drivers of these modeled trend biases, the ESM4, and CM4 forcing subset experiments (GHG, AA, and natural forcing-only runs) are analyzed. The assessment confirms the generally negative and positive contributions of AA and GHG forcings, respectively, to the long-term NH land precipitation changes.

The zonal mean historical precipitation change difference vs. observations (derived from the model all-forcing precipitation anomaly minus the observed anomaly from their respective 1915-1945 reference values) shows a clear temporal consistency in evolution between the model-observation differences and the evolution of precipitation anomalies in the aerosol-only experiments. For 15°–45° N zonal mean and the region of East Asia, the all-forcing models' precipitation differences vs. observations increase at the century scale; For

36

45°–80° N and northern Europe, the precipitation differences reach their peak value around the 1970s and have decreased slightly since. The model-observation precipitation differences are particularly well-correlated with the evolution of AA emissions, burdens, and modeled response over Europe and East Asia. The result suggests the overestimation of AA forcing or aerosol-related model response as a potential cause of the negative bias of the ESM4 and CM4 historical precipitation century-scale trends.

Apart from anthropogenic forcings, land precipitation changes are also influenced by SST changes, as demonstrated by comparing observations, all-forcing simulations, and LongAMIP simulations forced by radiative forcings and observed sea surface temperature and sea ice variations. In tropical land regions (15°S–15°N and West Africa), SST influences help reduce the models' historical precipitation change differences vs. observations, suggesting that uncaptured forced SST variability as well as internal multidecadal SST variability may play critical roles in the discrepancy between model precipitation simulations and observations. However, for higher latitudes (15–45°N and 45–80°N), SST was found to be a less dominant factor than anthropogenic forcings and related model responses in producing the simulation discrepancies since the 1960s.Previous work indicates the impacts of AAs and GHGs on precipitation through various mechanisms, and a correlated response between regional precipitation and T_s changes has been highlighted. In this paper, we analyze the observed and modeled long-term temperature changes to further investigate the possible contributions of external forcings to the modeled temperature and precipitation biases collectively. The temperature trend maps show that, compared to the observation (BEST), the ESM4 and CM4 all-forcing runs depict a weaker increasing trend of T_s over land regions of middle-high latitudes NH, and an unrealistic cooling tendency over East Asia. The ESM4 and CM4 T_s trend bias can be partially explained by the anomalous cooling during ~1950–1980 in the NH, predominantly driven by the aerosol forcing in the models. This overestimated cooling period is not only exhibited by the GFDL models but also found in other CMIP6 ESMs, which has been attributed to the high AA level in these models (Dittus et al., 2020; Zhang et al.,2021).

The underestimated surface air warming over land in the ESM4 and CM4 all-forcing simulations shows a spatial-temporal consistency with the models' precipitation trend bias. The relationship between the model trend biases in temperature and precipitation, and their consistency with the evolving aerosol forcing suggest the models' precipitation trend biases over the NH land could be caused by the overestimated aerosol dimming and cooling. This phenomenon is particularly significant in regions that had or still have high levels of air pollution and aerosol burdens (such as Europe and Asia).

Besides the model-observation difference, the all-forcing and forcing subset runs also show evident discrepancies in precipitation and T_s between ESM4 and CM4, which can be partially explained by the different positive contributions of the GHG response in the two models. Thus, the apparent underestimated moistening bias of ESM4 and CM4 in their century-scale historical trends over land regions could be caused by a combination of overestimated anthropogenic aerosol forcing/response and underestimated positive GHG forcing.

It is also possible that observational uncertainties and problems, including changes in observing practices, could contribute to the discrepancies we find, although the relatively coherent (though spatially sparse in some regions) increasing signal in the northern mid-to-high latitudes suggests a real precipitation-increasing trend signal in the observations, as opposed to a wide-spread – and spatially coherent – spurious trend artifact.

However, many of the above findings on trends from our work currently do not apply equally to the Southern Hemisphere. This could be attributable to **1)** the relatively low aerosol loading in the SH and **2)** the predominant effects of SST on the precipitation evolution over land regions, such as West Africa and Argentina. Our regional results illustrate the more spatially complex relationships between precipitation and long-term warming trends at small scales.

The underestimation of the century-scale trends of land precipitation in higher latitudes discussed in our study is not only exhibited by the two GFDL's climate models but is also

38

indicated to be an important issue for larger samples of CMIP5 and CMIP6 models (Knutson and Zeng, 2018; Vicente‑Serrano et al., 2021). Uncertainties in the AA forcing and response in climate models are also discussed by many previous studies (e.g., Stevens, 2013, 2015; Thorsen et al., 2020; Smith et al., 2021). Based on our analysis, we speculate that the various climate sensitivities to the aerosol and GHG forcings and the range of aerosol loading changes among current climate models may cause a large spread in historical trends and projections across these models and thus to uncertainties in their precipitation projections. Though only two GFDL models are employed in this paper, the precipitation trends and biases for other models in the CMIP6 dataset will be analyzed in a follow-up study. We hope this study and our follow-on work can provide some pathways for improvement of the CM4 and ESM4 models and their successor GFDL models, as well as historical climate simulations and projections using other models.

Data availability statement

The GPCC V6 monthly dataset is maintained by the Deutscher Wetterdienst, German Weather Service under the auspices of the World Meteorological Organization (WMO), available at https://www.esrl.noaa.gov/psd/data/gridded/data.gpcc.html; The Berkeley Earth land/ocean temperature product (BEST) data is available at monthly resolution for 1850-present at a $1° \times 1°$ spatial resolution available at http://berkeleyearth.org/data/. The ESM4 simulations and CM4 historical all-forcing and natural simulations are available in the CMIP6 archive. Requests for data from the CM4 forcing subset and LongAMIP specified SST/sea ice simulations used in the study should be directed to the authors.

References

Adcroft, A., and Coauthors, 2019: The GFDL global ocean and sea ice model OM4. 0: Model description and simulation features. *J. Adv. Model. Earth Syst.*, **11** (10), 3167–3211, https://doi.org/10.1029/2019MS001726

Allen, M. R., and W. J. Ingram, 2002: Constraints on future changes in climate and the hydrologic cycle. *Nature*, **419** (6903), 228–232, https://doi.org/10.1038/nature01092.

Allen, R.J., J.R. Norris, and M. Kovilakam, 2014: Influence of anthropogenic aerosols and the Pacific Decadal Oscillation on tropical belt width. *Nat. Geosci.*, **7**(4), 270–274, doi:10.1038/ngeo2091.

Allen, R.J., A.T. Evan, and B.B.B. Booth, 2015: Interhemispheric aerosol radiative forcing and tropical precipitation shifts during the late twentieth century. *J. Climate*, **28**(20), 8219–8246, doi:10.1175/jcli-d-15-0148.1.

Andrews, T., P. M. Forster, O. Boucher, N. Bellouin, and A. Jones, 2010: Precipitation, radiative forcing and global temperature change. *Geophys. Res. Lett.*, **37** (14), https://doi.org/10.1029/2010GL043991

Ayantika, D.C., Krishnan, R., Singh, M., Swapna, P., Sandeep, N., Prajeesh, A.G. and Vellore, R., 2021. Understanding the combined effects of global warming and anthropogenic aerosol forcing on the South Asian monsoon. *Climate Dyn.*, **56,** 1643-1662, doi:10.1007/s00382-020-05551-5

Bala, G., K. Caldeira, and R. Nemani, 2010: Fast versus slow response in climate change: implications for the global hydrological cycle. *Climate Dyn.*, **35**(2–3), 423–434, doi:10.1007/s00382-009-0583-y.

Becker, A., Finger, P., Meyer-Christoffer, A., Rudolf, B., Schamm, K., Schneider, U. and Ziese, M., 2013. A description of the global land-surface precipitation data products of the Global Precipitation Climatology Centre with sample applications including centennial (trend) analysis from 1901–present. *Earth Syst. Sci. Data*, **5**(1), pp.71-99. https://doi.org/10.5194/essd-5-71-2013

Bollasina, M. A., Ming, Y., & Ramaswamy, V., 2011: Anthropogenic aerosols and the weakening of the South Asian summer monsoon. *Science*, **334**(6055), 502-505. https://www.science.org/doi/10.1126/science.1204994

Boer, G., 1993: Climate change and the regulation of the surface moisture and energy budgets. *Climate Dyn.*, **8** (5), 225–239.

Bonfils, C.J., Santer, B.D., Fyfe, J.C., Marvel, K., Phillips, T.J. and Zimmerman, S.R., 2020: Human influence on joint changes in temperature, rainfall and continental aridity. *Nat. Climate Change*, **10**(8), 1–6, doi:10.1038/s41558-020-0821-1.

Brönnimann, S., Fischer, A.M., Rozanov, E., Poli, P., Compo, G.P. and Sardeshmukh, P.D., 2015: Southward shift of the northern tropical belt from 1945 to 1980. *Nat. Geosci.*, **8**(12), 969–974, doi:10.1038/ngeo2568.

Bryant, R.G., Bigg, G.R., Mahowald, N.M., Eckardt, F.D. and Ross, S.G., 2007. Dust emission response to climate in southern Africa. *J. Geophys. Res.*, 112(D9). https://doi.org/10.1029/2005JD007025.

Cao, L., G. Bala, and K. Caldeira, 2012: Climate response to changes in atmospheric carbon dioxide and solar irradiance on the time scale of days to weeks. *Environ. Res. Lett.*, **7**(3), 34015, doi:10.1088/1748-9326/7/3/034015.

Carslaw, K.S., Boucher, O., Spracklen, D.V., Mann, G.W., Rae, J.G.L., Woodward, S. and Kulmala, M., 2010. A review of natural aerosol interactions and feedbacks within the Earth system. *Atmos. Chem. Phys.*, **10**(4), pp.1701-1737. https://doi.org/10.5194/acp-10-1701-2010

Chou, C., and J. D. Neelin, 2004: Mechanisms of global warming impacts on regional tropical precipitation. *J. Climate*, **17** (13), 2688–2701, https://doi.org/10.1175/1520-0442(2004)017<2688:MOGWIO>2.0.CO;2

Chou, C., J. D. Neelin, C.-A. Chen, and J.-Y. Tu, 2009: Evaluating the "rich-get-richer" mechanism in tropical precipitation change under global warming. *J. Climate*, **22** (8), 1982–2005, https://doi.org/10.1175/2008JCLI2471.1

Chou, C., J. D. Neelin, J.-Y. Tu, and C.-T. Chen, 2006: Regional tropical precipitation change mechanisms in ECHAM4/OPYC3 under global warming. *J. Climate*, **19** (17), 4207–4223, https://doi.org/10.1175/JCLI3858.1

Christidis, N., & Stott, P. A. (2022). Human influence on seasonal precipitation in Europe. *J. Climate,* **35**(15), 5215-5231. https://doi.org/10.1175/JCLI-D-21-0637.1

Collins, M., and Coauthors, 2013: Long-term climate change: projections, commitments and irreversibility. In *Climate Change 2013-The Physical Science Basis: Contribution of Working Group I to the Fifth Assessment Report of the Intergovernmental Panel on Climate Change,* Cambridge University Press, 1029–1136.

Dai, A. and Bloecker, C.E., 2019. Impacts of internal variability on temperature and precipitation trends in large ensemble simulations by two climate models. *Climate Dyn.*, **52**(1-2), pp.289-306. https://doi.org/10.1007/s00382-018-4132-4

Dai, A., and T. Zhao, 2017: Uncertainties in historical changes and future projections of drought. part i: estimates of historical drought changes. *Climatic Change*, 144 (3), 519–533, https://doi.org/10.1007/s10584-016-1705-2

Delworth, T.L. and F. Zeng, 2014: Regional rainfall decline in Australia attributed to anthropogenic greenhouse gases and ozone levels. *Nat. Geosci.*, 7(8), 583–587, doi:10.1038/ngeo2201.

Deser, C., Knutti, R., Solomon, S. and Phillips, A.S., 2012. Communication of the role of natural variability in future North American climate. *Nat. Climate Change*, **2**(11), pp.775-779，doi:10.1038/nclimate1562

Dirmeyer, P. A., Y. Jin, B. Singh, and X. Yan, 2013: Evolving land–atmosphere interactions over North America from CMIP5 simulations. *J. Climate,* **26** (19), 7313–7327, https://doi.org/10.1175/JCLI-D-12-00454.1

Dittus, A. J., Hawkins, E., Wilcox, L. J., Sutton, R. T., Smith, C. J., Andrews, M. B., & Forster, P. M., 2020: Sensitivity of historical climate simulations to uncertain aerosol

forcing. *Geophys. Res. Lett.*, **47**(13), e2019GL085806.
https://doi.org/10.1029/2019GL085806

Dong, B., and R. Sutton, 2015: Dominant role of greenhouse-gas forcing in the recovery of
Sahel rainfall. *Nat. Climate Change*, **5** (8), 757–760,
https://doi.org/10.1038/nclimate2664

Douville, H., K. Raghavan, J. Renwick, R.P. Allan, P.A. Arias, M. Barlow, R. Cerezo-Mota,
A. Cherchi, T.Y. Gan, J. Gergis, D. Jiang, A. Khan, W. Pokam Mba, D. Rosenfeld, J.
Tierney, and O. Zolina, 2021: Water cycle changes. In *Climate Change 2021: The
Physical Science Basis. Contribution of Working Group I to the Sixth Assessment
Report of the Intergovernmental Panel on Climate Change* [Masson-Delmotte, V., P.
Zhai, A. Pirani, S.L. Connors, C. Péan, S. Berger, N. Caud, Y. Chen, L. Goldfarb,
M.I. Gomis, M. Huang, K. Leitzell, E. Lonnoy, J.B.R. Matthews, T.K. Maycock, T.
Waterfield, O. Yelekçi, R. Yu, and B. Zhou (eds.)]. Cambridge University Press,
Cambridge, United Kingdom and New York, NY, USA, pp. 1055–1210,
doi:10.1017/9781009157896.010.

Dunne, J., and Coauthors, 2020: The GFDL Earth System Model Version 4.1 (GFDL-ESM
4.1): Overall coupled model description and simulation characteristics. *J. Adv. Model.
Earth Syst.*, 12 (11), e2019MS002 015. https://doi.org/10.1029/2019MS002015

Eyring, V., S. Bony, G. A. Meehl, C. A. Senior, B. Stevens, R. J. Stouffer, and K. E. Taylor,
2016: Overview of the Coupled Model Intercomparison Project Phase 6 (CMIP6)
experimental design and organization. *Geosci. Model Dev.*, **9** (5), 1937–1958 ,
https://doi.org/10.5194/gmd-9-1937-2016, 2016

Fläschner, D., T. Mauritsen, and B. Stevens, 2016: Understanding the intermodel spread in
global-mean hydrological sensitivity. *J. Climate*, **29**(2), 801–817, doi:10.1175/jcli-d-
15-0351.1.

Fyfe, J., N. Gillett, and G. Marshall, 2012: Human influence on extratropical southern
hemisphere summer precipitation. *Geophys. Res. Lett.*, **39**
(23), https://doi.org/10.1029/2012GL054199

Giorgi, F., and X. Bi, 2005: Updated regional precipitation and temperature changes for the 21st century from ensembles of recent AOGCM simulations. *Geophys. Res. Lett*., **32** (21), https://doi.org/10.1029/2005GL024288.

Greve, P., B. Orlowsky, B. Mueller, J. Sheffield, M. Reichstein, and S. I. Seneviratne, 2014: Global assessment of trends in wetting and drying over land. *Nat. Geosci*., **7** (10), 716–721, https://doi.org/10.1038/ngeo2247

Gu, G., Adler, R. F., and Huffman, G. J. (2016). Long-term changes/trends in surface temperature and precipitation during the satellite era (1979–2012). *Climate Dyn*., **46**, 1091-1105. https://doi.org/10.1007/s00382-015-2634-x

Guo, L., Highwood, E. J., Shaffrey, L. C., and Turner, A. G., 2013: The effect of regional changes in anthropogenic aerosols on rainfall of the East Asian Summer Monsoon, *Atmos. Chem. Phys*., **13**, 1521–1534, https://doi.org/10.5194/acp-13-1521-2013.

Guo, Huan; John, Jasmin G; Blanton, Chris; McHugh, Colleen; Nikonov, Serguei; Radhakrishnan, Aparna; Rand, Kristopher; Zadeh, Niki T.; Balaji, V; Durachta, Jeff; Dupuis, Christopher; Menzel, Raymond; Robinson, Thomas; Underwood, Seth; Vahlenkamp, Hans; Bushuk, Mitchell; Dunne, Krista A.; Dussin, Raphael; Gauthier, Paul PG; Ginoux, Paul; Griffies, Stephen M.; Hallberg, Robert; Harrison, Matthew; Hurlin, William; Lin, Pu; Malyshev, Sergey; Naik, Vaishali; Paulot, Fabien; Paynter, David J; Ploshay, Jeffrey; Reichl, Brandon G; Schwarzkopf, Daniel M; Seman, Charles J; Shao, Andrew; Silvers, Levi; Wyman, Bruce; Yan, Xiaoqin; Zeng, Yujin; Adcroft, Alistair; Dunne, John P.; Held, Isaac M; Krasting, John P.; Horowitz, Larry W.; Milly, P.C.D; Shevliakova, Elena; Winton, Michael; Zhao, Ming; Zhang, Rong, 2018: NOAA-GFDL GFDL-CM4 model output historical. Earth System Grid Federation, accessed 04 January 2022, https://doi.org/10.22033/ESGF/CMIP6.8594

Hamed, K. H., and A. R. Rao, 1998: A modified Mann-Kendall trend test for autocorrelated data. *J. Hydrology*, 204 (1-4), 182–196, https://doi.org/10.1016/S0022-1694(97)00125-X

Hartmann, D. L., and Coauthors, 2013: Observations: atmosphere and surface. *Climate Change 2013, The Physical Science Basis: Working Group I Contribution to the Fifth Assessment Report of the Intergovernmental Panel on Climate Change,* Cambridge University Press, 159–254.

Harris, I.P.D.J., Jones, P.D., Osborn, T.J. and Lister, D.H., 2014. Updated high- resolution grids of monthly climatic observations–the CRU TS3.10 dataset. *Int. J. Climatology*, 34(3), pp.623-642, https://doi.org/10.1002/joc.3711

Hawkins, E., and R. Sutton, 2009: The potential to narrow uncertainty in regional climate predictions. *Bull. Amer. Meteor. Soc.*, **90** (8), 1095–1108, https://doi.org/10.1175/2009BAMS2607.1

Hawkins, E., and R. Sutton, 2011: The potential to narrow uncertainty in projections of regional precipitation change. *Climate Dyn.,* **37** (1), 407–418, https://doi.org/10.1007/s00382-010-0810-6

Held, I., and Coauthors, 2019: Structure and performance of GFDL's CM4. 0 climate model. *J. Adv. Model. Earth Syst.*, **11** (11), 3691–3727, https://doi.org/10.1029/2019MS001829

Held, I. M., T. L. Delworth, J. Lu, K. Findell, and T. Knutson, 2005: Simulation of Sahel drought in the 20th and 21st centuries. *Proc. Natl. Acad. Sci.*, **102** (50), 17 891–17 896, https://doi.org/10.1073/pnas.0509057102

Held, I. M., and B. J. Soden, 2006: Robust responses of the hydrological cycle to global warming. *J. Climate*, **19** (21), 5686–5699, https://doi.org/10.1175/JCLI3990.1

Hoerling, M., J. Hurrell, J. Eischeid, and A. Phillips, 2006: Detection and attribution of twentieth-century northern and southern African rainfall change. *J. Climate*, **19** (16), 3989–4008, https://doi.org/10.1175/JCLI3842.1

Hoerling, M., Eischeid, J., Perlwitz, J., Quan, X., Zhang, T. and Pegion, P., 2012: On the increased frequency of Mediterranean drought. *J. Climate,* **25**(6), 2146–2161, doi:10.1175/jcli-d-11-00296.1.

Horowitz, Larry W.; John, Jasmin G.; Blanton, Chris; McHugh, Colleen; Radhakrishnan, Aparna; Rand, Kristopher; Vahlenkamp, Hans; Zadeh, Niki T.; Wilson, Chandin; Dunne, John P.; Ploshay, Jeffrey; Winton, Michael; Zeng, Yujin, 2018: NOAA-GFDL GFDL-ESM4 model output prepared for CMIP6 DAMIP hist-GHG, Earth System Grid Federation, accessed 04 January 2022, https://doi.org/10.22033/ESGF/CMIP6.8570

Horowitz, Larry W.; John, Jasmin G.; Blanton, Chris; McHugh, Colleen; Radhakrishnan, Aparna; Rand, Kristopher; Vahlenkamp, Hans; Zadeh, Niki T.; Wilson, Chandin; Dunne, John P.; Ploshay, Jeffrey; Winton, Michael; Zeng, Yujin, 2018: NOAA-GFDL GFDL-ESM4 model output prepared for CMIP6 DAMIP hist-aer, Earth System Grid Federation, accessed 04 January 2022, https://doi.org/10.22033/ESGF/CMIP6.8571

Horowitz, Larry W.; John, Jasmin G.; Blanton, Chris; McHugh, Colleen; Radhakrishnan, Aparna; Rand, Kristopher; Vahlenkamp, Hans; Zadeh, Niki T.; Wilson, Chandin; Dunne, John P.; Ploshay, Jeffrey; Winton, Michael; Zeng, Yujin, 2018: NOAA-GFDL GFDL-ESM4 model output prepared for CMIP6 DAMIP hist-nat, Earth System Grid Federation, accessed 04 January 2022, https://doi.org/10.22033/ESGF/CMIP6.8575

IPCC, 2013: *Climate Change 2013: The Physical Science Basis. Contribution of Working Group I to the Fifth Assessment Report of the Intergovernmental Panel on Climate Change* [Stocker, T.F., D. Qin, G.-K. Plattner, M. Tignor, S.K. Allen, J. Boschung, A. Nauels, Y. Xia, V. Bex and P.M. Midgley (eds.)]. Cambridge University Press, Cambridge, United Kingdom and New York, NY, USA, 1535 pp.

IPCC, 2014: *Climate Change 2014: Synthesis Report. Contribution of Working Groups I, II and III to the Fifth Assessment Report of the Intergovernmental Panel on Climate Change* [Core Writing Team, R.K. Pachauri, and L.A. Meyer(eds.)]. IPCC, Geneva, Switzerland, 151 pp., www.ipcc.ch/report/ar5/syr.

IPCC, 2021*: Summary for Policymakers. In: Climate Change 2021: The Physical Science Basis. Contribution of Working Group I to the Sixth Assessment Report of the Intergovernmental Panel on Climate Change* [Masson-Delmotte, V., P. Zhai, A.

Pirani, S. L. Connors, C. Péan, S. Berger, N. Caud, Y. Chen, L.Goldfarb, M. I. Gomis, M. Huang, K. Leitzell, E. Lonnoy, J.B.R. Matthews, T. K. Maycock, T. Waterfield,O. Yelekçi, R. Yu and B. Zhou (eds.)]. Cambridge University Press, Cambridge, United Kingdom and New York, NY, USA, pp. 3−32, doi:10.1017/9781009157896.001.

Knutson, T. R., and J. Ploshay, 2021: Sea level pressure trends: Model-based assessment of detection, attribution, and consistency with CMIP5 historical simulations. *J. Climate*, **34** (1), 327–346, https://doi.org/10.1175/JCLI-D-19-0997.1

Knutson, T. R., and F. Zeng, 2018: Model assessment of observed precipitation trends over land regions: detectable human influences and possible low bias in model trends. *J. Climate*, **31** (12), 4617–4637, https://doi.org/10.1175/JCLI-D-17-0672.1

Knutson, T. R., F. Zeng, and A. T. Wittenberg, 2013: Multimodel assessment of regional surface temperature trends: CMIP3 and CMIP5 twentieth-century simulations. *J. Climate*, **26** (22), 8709–8743, https://doi.org/10.1175/JCLI-D-12-00567.1

Kok, J.F., Storelvmo, T., Karydis, V.A., Adebiyi, A.A., Mahowald, N.M., Evan, A.T., He, C. and Leung, D.M., 2023. Mineral dust aerosol impacts on global climate and climate change. *Nat. Rev. Earth & Envir.*, pp.1-16. https://doi.org/10.1038/s43017-022-00379-5

Krasting, John P.; John, Jasmin G; Blanton, Chris; McHugh, Colleen; Nikonov, Serguei; Radhakrishnan, Aparna; Rand, Kristopher; Zadeh, Niki T.; Balaji, V; Durachta, Jeff; Dupuis, Christopher; Menzel, Raymond; Robinson, Thomas; Underwood, Seth; Vahlenkamp, Hans; Dunne, Krista A.; Gauthier, Paul PG; Ginoux, Paul; Griffies, Stephen M.; Hallberg, Robert; Harrison, Matthew; Hurlin, William; Malyshev, Sergey; Naik, Vaishali; Paulot, Fabien; Paynter, David J; Ploshay, Jeffrey; Reichl, Brandon G; Schwarzkopf, Daniel M; Seman, Charles J; Silvers, Levi; Wyman, Bruce; Zeng, Yujin; Adcroft, Alistair; Dunne, John P.; Dussin, Raphael; Guo, Huan; He, Jian; Held, Isaac M; Horowitz, Larry W.; Lin, Pu; Milly, P.C.D; Shevliakova, Elena; Stock, Charles; Winton, Michael; Wittenberg, Andrew T.; Xie, Yuanyu; Zhao, Ming

2018: NOAA-GFDL GFDL-ESM4 model output prepared for CMIP6 CMIP historical, Earth System Grid Federation, accessed 04 January 2022, https://doi.org/10.22033/ESGF/CMIP6.8597

Krishnan, R., Sabin, T.P., Vellore, R., Mujumdar, M., Sanjay, J., Goswami, B.N., Hourdin, F., Dufresne, J.L. and Terray, P., 2016: Deciphering the desiccation trend of the South Asian monsoon hydroclimate in a warming world. *Climate Dyn.*, **47**(3–4), 1007–1027, doi:10.1007/s00382-015-2886-5

Knutti, R., and J. Sedláček, 2013: Robustness and uncertainties in the new CMIP5 climate model projections. *Nat. Climate Change*, **3** (4), 369–373, https://doi.org/10.1038/nclimate1716

Kumar, S., V. Merwade, J. L. Kinter III, and D. Niyogi, 2013: Evaluation of temperature and precipitation trends and long-term persistence in CMIP5 twentieth-century climate simulations. *J. Climate*, **26** (12), 4168–4185, https://doi.org/10.1175/JCLI-D-12-00259.1

Lau, W.K.-M. and K.-M. Kim, 2017: Competing influences of greenhouse warming and aerosols on Asian summer monsoon circulation and rainfall. *Asia-Pacific J. Atmos. Sci.*, 53(2), 181–194, doi:10.1007/s13143-017-0033-4.

Lin, L., Xu, Y., Wang, Z., Diao, C., Dong, W., & Xie, S. P., 2018: Changes in extreme rainfall over India and China attributed to regional aerosol- cloud interaction during the late 20th century rapid industrialization. *Geophys. Res. Lett.*, **45**(15), 7857-7865. https://doi.org/10.1029/2018GL078308

Li, Z., Lau, W. M., Ramanathan, V., Wu, G., Ding, Y., Manoj, M. G., ... & Brasseur, G. P., 2016: Aerosol and monsoon climate interactions over Asia. *Rev. Geophys.*, **54**(4), 866-929. https://doi.org/10.1002/2015RG000500

Liu, C., and Allan, R. P. (2013). Observed and simulated precipitation responses in wet and dry regions 1850–2100. *Environ. Res. Lett.*, **8**(3), 034002. https://doi.org/10.1088/1748-9326/8/3/034002

Liu, J., B. Wang, M. A. Cane, S.-Y. Yim, and J.-Y. Lee, 2013: Divergent global precipitation changes induced by natural versus anthropogenic forcing. *Nature,* **493** (7434), 656–659, https://doi.org/10.1038/nature11784

Mahlstein, I., R. W. Portmann, J. S. Daniel, S. Solomon, and R. Knutti, 2012: Perceptible changes in regional precipitation in a future climate. *Geophys. Res. Lett.,* **39** (5). https://doi.org/10.1029/2011GL050738

Marvel, K., and C. Bonfils, 2013: Identifying external influences on global precipitation. *Proc. Natl. Acad. Sci.*, **110** (48), 19 301–19 306, https://doi.org/10.1073/pnas.1314382110

Meehl, G. A., C. Covey, T. Delworth, M. Latif, B. McAvaney, J. F. Mitchell, R. J. Stouffer, and K. E. Taylor, 2007: The WCRP CMIP3 multimodel dataset: A new era in climate change research. *Bull. Amer. Meteor. Soc.*, **88** (9), 1383–1394, http://dx.doi.org/10.1175/BAMS-88-9-1383

Min, S.-K., X. Zhang, F. W. Zwiers, and T. Agnew, 2008: Human influence on Arctic sea ice detectable from early 1990s onwards. *Geophys. Res. Lett.*, **35** (21), https://doi.org/10.1029/2008GL035725

Mitchell, J. F., C. Wilson, and W. Cunnington, 1987: On CO2 climate sensitivity and model dependence of results. *Quart. J. Roy. Meteor. Soc.*, **113** (475), 293–322, https://doi.org/10.1002/qj.49711347517

Nasrollahi, N., A. AghaKouchak, L. Cheng, L. Damberg, T. J. Phillips, C. Miao, K. Hsu, and S. Sorooshian, 2015: How well do CMIP5 climate simulations replicate historical trends and patterns of meteorological droughts? *Water Resour. Res.*, 51 (4), 2847–2864, https://doi.org/10.1002/2014WR016318

Neelin, J., C. Chou, and H. Su, 2003: Tropical drought regions in global warming and El Niño teleconnections. *Geophys. Res. Lett.*, **30** (24), https://doi.org/10.1029/2003GL018625

Orlowsky, B., and S. I. Seneviratne, 2012: Global changes in extreme events: regional and seasonal dimension. *Climatic Change*, **110** (3), 669–696, https://doi.org/10.1007/s10584-011-0122-9

Orlowsky, B., and S. I. Seneviratne, 2013: Elusive drought: uncertainty in observed trends and short-and long-term CMIP5 projections. *Hydrol. Earth Syst. Sci.,* 17 (5), 1765–1781, https://doi.org/10.5194/hess-17-1765-2013

O'Gorman, P. A., R. P. Allan, M. P. Byrne, and M. Previdi, 2012: Energetic constraints on precipitation under climate change. *Surv. Geophys.*, 33 (3), 585–608, https://doi.org/10.1007/s10712-011-9159-6

Paulot, F., D. Paynter, M. Winton, P. Ginoux, M. Zhao, and L. W. Horowitz, 2020: Revisiting the impact of sea salt on climate sensitivity. *Geophys. Res. Lett*., **47** (3), e2019GL085 601. https://doi.org/10.1029/2019GL085601

Ploshay, Jeffrey; Hurlin, William; John, Jasmin G; Blanton, Chris; McHugh, Colleen; Radhakrishnan, Aparna; Rand, Kristopher; Vahlenkamp, Hans; Zadeh, Niki T.; Wilson, Chandin; Paynter, David J; Winton, Michael; Zeng, Yujin; Knutson, Thomas, 2018: NOAA-GFDL GFDL-CM4 model output prepared for CMIP6 DAMIP hist-nat, Earth System Grid Federation, accessed 04 January 2022, https://doi.org/10.22033/ESGF/CMIP6.11330

Polson, D., M. Bollasina, G. C. Hegerl, and L. Wilcox, 2014: Decreased monsoon precipitation in the northern hemisphere due to anthropogenic aerosols. *Geophys. Res. Lett*., **41** (16), 6023–6029, https://doi.org/10.1002/2014GL060811

Previdi, M., 2010: Radiative feedbacks on global precipitation. *Envir. Res. Lett*., 5 (2), 025 211, https://doi.org/10.1088/1748-9326/5/2/025211

Raäisaänen, J., 2007: How reliable are climate models? *Tellus*, **59** (1), 2–29, https://doi.org/10.1111/j.1600-0870.2006.00211.x

Ren, L., P. Arkin, T. M. Smith, and S. S. Shen, 2013: Global precipitation trends in 1900–2005 from a reconstruction and coupled model simulations. *J. Geophys. Res.*, 118 (4), 1679–1689, https://doi.org/10.1002/jgrd.50212

Rohde, R., and Coauthors, 2013a: A new estimate of the average earth surface land temperature spanning 1753 to 2011. *Geoinfor. Geostat.: An Overview* 1: 1, http://dx.doi.org/10.4172/2327-4581.1000101

Rohde, R., and Coauthors, 2013b: Berkeley Earth temperature averaging process,. *Geoinfor. Geostat.: An Overview*, **1** (2), 20–100, http://dx.doi.org/10.4172/gigs.1000103

Rotstayn, L.D., U. Lohmann, L.D. Rotstayn, and U. Lohmann, 2002: Tropical rainfall trends and the indirect aerosol effect. *J. Climate,* **15**(15), 2103–2116, doi:10.1175/1520-0442(2002)015<2103:trtati>2.0.co;2.

Rowell, D. P., 2012: Sources of uncertainty in future changes in local precipitation. *Climate Dyn.,* **39** (7), 1929–1950, https://doi.org/10.1007/s00382-011-1210-2

Samset BH, Myhre G, Forster PM, Hodnebrog Ø, Andrews T, Faluvegi G, Flaeschner D, Kasoar M, Kharin V, Kirkevåg A, Lamarque JF., 2016: Fast and slow precipitation responses to individual climate forcers: A PDRMIP multimodel study. *Geophys. Res. Lett*., **43**(6), 2782–2791, doi:10.1002/2016gl068064

Samset BH, Sand M, Smith CJ, Bauer SE, Forster PM, Fuglestvedt JS, Osprey S, Schleussner CF. 2018: Climate impacts from a removal of anthropogenic aerosol emissions. *Geophys. Res. Lett*., **45**(2), 1020–1029, doi:10.1002/2017gl076079..

Sanap, S.D., G. Pandithurai, and M.G. Manoj, 2015: On the response of Indian summer monsoon to aerosol forcing in CMIP5 model simulations. *Climate Dyn*., **45**(9–10), 2949–2961, doi:10.1007/s00382-015-2516-2.

Sellar, A. A., Jones, C. G., Mulcahy, J. P., Tang, Y., Yool, A., Wiltshire, A., ... & Zerroukat, M., 2019: UKESM1: Description and evaluation of the UK Earth System Model. *J. Adv. Model. Earth Syst.*, **11**(12), 4513-4558, https://doi.org/10.1029/2019MS001739

Schneider, Udo; Becker, Andreas; Finger, Peter; Rustemeier, Elke; Ziese, Markus (2020): GPCC Full Data Monthly Product Version 2020 at 2.5°: Monthly Land-Surface Precipitation from Rain-Gauges built on GTS-based and Historical Data. https://doi.org/10.5676/DWD_GPCC/FD_M_V2020_250

Smith, C. J., and Coauthors, 2021: Energy budget constraints on the time history of aerosol forcing and climate sensitivity. *J. Geophys. Res.: Atmos*., **126** (13), e2020JD033 622, https://doi.org/10.1029/2020JD033622

Stevens, B., 2013: Uncertain then, irrelevant now. *Nature*, **503** (7474), 47–48, https://doi.org/10.1038/503047a

Stevens, B., 2015: Rethinking the lower bound on aerosol radiative forcing. *J. Climate*, **28** (12), 4794–4819, https://doi.org/10.1175/JCLI-D-14-00656.1

Taylor, K. E., R. J. Stouffer, and G. A. Meehl, 2012: An overview of CMIP5 and the experiment design. *Bull. Amer. Meteor. Soc*., **93** (4), 485–498. https://doi.org/10.1175/BAMS-D-11-00094.1

Trenberth, K. E., 2011: Changes in precipitation with climate change. *Climate Res*., **47** (1-2), 123–138, https://doi.org/10.3354/cr00953

Thorsen, T. J., R. A. Ferrare, S. Kato, and D. M. Winker, 2020: Aerosol direct radiative effect sensitivity analysis. *J. Climate*, **33** (14), 6119–6139. https://doi.org/10.1175/JCLI-D-19-0669.1

Undorf, S., Polson, D., Bollasina, M.A., Ming, Y., Schurer, A. and Hegerl, G.C., 2018: Detectable impact of local and remote anthropogenic aerosols on the 20th century changes of West African and South Asian monsoon precipitation. *J. Geophys. Res.*, **123**(10), 4871–4889, doi:10.1029/2017jd027711.

Van Oldenborgh, G. J., F. D. Reyes, S. Drijfhout, and E. Hawkins, 2013: Reliability of regional climate model trends. *Environ. Res. Lett*., 8 (1), 014 055. https://doi.org/10.1088/1748-9326/8/1/014055

Vecchi, G. A., and B. J. Soden, 2007: Global warming and the weakening of the tropical circulation. *J. Climate*, **20** (17), 4316–4340. https://doi.org/10.1175/JCLI4258.1

Vicente-Serrano, S., and Coauthors, 2022: Do CMIP models capture long-term observed annual precipitation trends? *Climate Dyn.,* **58** (9), 2825–2842. https://doi.org/10.1007/s00382-021-06034-x

Wan, H., X. Zhang, F. Zwiers, and S.-K. Min, 2015: Attributing northern high-latitude precipitation change over the period 1966–2005 to human influence. *Climate Dyn*., **45** (7), 1713–1726, https://doi.org/10.1007/s00382-014-2423-y

Wilcox, L. J., E. J. Highwood, and N. J. Dunstone, 2013: The influence of anthropogenic aerosol on multi-decadal variations of historical global climate. *Environ. Res. Lett*., **8** (2), 024 033. https://doi.org/10.1088/1748-9326/8/2/024033

Wilcox, L. J., Liu, Z., Samset, B. H., Hawkins, E., Lund, M. T., Nordling, K., Undorf, S., Bollasina, M., Ekman, A. M. L., Krishnan, S., Merikanto, J., and Turner, A. G., 2020: Accelerated increases in global and Asian summer monsoon precipitation from future aerosol reductions, *Atmos. Chem. Phys*., **20**, 11955–11977, https://doi.org/10.5194/acp-20-11955-2020.

Wild, M., 2012: Enlightening global dimming and brightening. *Bull. Amer. Meteor. Soc*., **93**(1), 27–37, doi:10.1175/bams-d-11-00074.1.

Yue, S., and C. Wang, 2004: The Mann-Kendall test modified by effective sample size to detect trend in serially correlated hydrological series. *Water Resour. Manag*., 18 (3), 201–218 doi:10.1023/B:WARM.0000043140.61082.60, https://doi.org/10.1023/B:WARM.0000043140.61082.60

Zeng, Y., Milly, P. C., Shevliakova, E., Malyshev, S., van Huijgevoort, M. H. J., and Dunne, K. A. (2022). Possible anthropogenic enhancement of precipitation in the Sahel-Sudan Savanna by remote agricultural irrigation. *Geophys. Res. Lett*., **49**(6), e2021GL096972. https://doi.org/10.1029/2021GL096972

Zhang, H., T. L. Delworth, F. Zeng, G. Vecchi, K. Paffendorf, and L. Jia, 2016: Detection, attribution, and projection of regional rainfall changes on (multi-) decadal time scales: A focus on southeastern South America. *J. Climate*, **29** (23), 8515–8534. https://doi.org/10.1175/JCLI-D-16-0287.1

Zhang, J., Furtado, K., Turnock, S. T., Mulcahy, J. P., Wilcox, L. J., Booth, B. B., Sexton, D., Wu, T., Zhang, F., and Liu, Q., 2021: The role of anthropogenic aerosols in the anomalous cooling from 1960 to 1990 in the CMIP6 earth system models, *Atmos. Chem. Phys.*, **21,** 18609–18627, https://doi.org/10.5194/acp-21-18609-2021.

Zhang, X., F. W. Zwiers, G. C. Hegerl, F. H. Lambert, N. P. Gillett, S. Solomon, P. A. Stott, and T. Nozawa, 2007: Detection of human influence on twentieth-century precipitation trends. *Nature,* **448** (7152), 461–465. https://doi.org/10.1038/nature06025

Zhao, M., and Coauthors, 2018a: The GFDL global atmosphere and land model AM4. 0/LM4. 0: 1. Simulation characteristics with prescribed SSTs. *J. Adv. Model. Earth Syst.*, **10** (3), 691–734, https://doi.org/10.1002/2017MS001208

Zhao, M., and Coauthors, 2018b: The GFDL global atmosphere and land model AM4. 0/LM4. 0: 2. Model description, sensitivity studies, and tuning strategies. *J. Adv. Model. Earth Syst.*, **10** (3), 735–769. https://doi.org/10.1002/2017MS001209

Zhao, T., L. Chen, and Z. Ma, 2014: Simulation of historical and projected climate change in arid and semiarid areas by CMIP5 models. *Chinese Sci. Bull.*, **59** (4), 412–429. https://doi.org/10.1007/s11434-013-0003-x

Zhang, Y., Luo, G., and Yu, F., 2019, Seasonal variations and long- term trend of dust particle number concentration over the northeastern United States. *J. Geophys. Res.,* **124**(23), 13140-13155. https://doi.org/10.1029/2019JD031388

Zhang, Y., Yu, F., Luo, G., Fan, J., and Liu, S., 2021, Impacts of long-range-transported mineral dust on summertime convective cloud and precipitation: a case study over the Taiwan region. *Atmos. Chem. Phys.*, **21**, 17433–17451, https://doi.org/10.5194/acp-21-17433-2021, 2021.